Comparison of Two Methods for Estimating the Sampling-Related Uncertainty of Satellite Rainfall Averages Based on a Large Radar Dataset

MATTHIAS STEINER

Department of Civil and Environmental Engineering, Princeton University, Princeton, New Jersey

THOMAS L. BELL

Laboratory for Atmospheres, NASA Goddard Space Flight Center, Greenbelt, Maryland

YU ZHANG AND ERIC F. WOOD

Department of Civil and Environmental Engineering, Princeton University, Princeton, New Jersey

(Manuscript received 22 October 2002, in final form 24 March 2003)

ABSTRACT

The uncertainty of rainfall estimated from averages of discrete samples collected by a satellite is assessed using a multiyear radar dataset covering a large portion of the United States. The sampling-related uncertainty of rainfall estimates is evaluated for all combinations of 100-, 200-, and 500-km space domains; 1-, 5-, and 30-day rainfall accumulations; and regular sampling time intervals of 1, 3, 6, 8, and 12 h. These extensive analyses are combined to characterize the sampling uncertainty as a function of space and time domain, sampling frequency, and rainfall characteristics by means of a simple scaling law. Moreover, it is shown that both parametric and nonparametric statistical techniques of estimating the sampling uncertainty produce comparable results. Sampling uncertainty estimates, however, do depend on the choice of technique for obtaining them. They can also vary considerably from case to case, reflecting the great variability of natural rainfall, and should therefore be expressed in probabilistic terms. Rainfall calibration errors are shown to affect comparison of results obtained by studies based on data from different climate regions and/or observation platforms.

1. Introduction

Monitoring rainfall on a global scale is key to a quantitative understanding of the global hydrologic cycle and our climate system. Observations from spaceborne platforms offer global coverage, albeit with limited sampling in space and time depending on the satellite's orbit and instrument configuration. This limitation in sampling frequency, in combination with the intermittence of rainfall in space and time, causes satellite-based rainfall estimates to be uncertain. Studies such as North and Nakamoto (1989), Bell et al. (1990), Steiner (1996), Bell and Kundu (2000), and Bell et al. (2001), using ground-based rainfall data, have shown that this uncertainty is expected to decrease for higher rainfall rates, larger domain sizes, and longer time integration. This has also been seen in studies using satellite data, for example, by Chang et al. (1993), Weng et al. (1994), Berg and Avery (1995), Huffman (1997), and Chang and Chiu (2001). On the other hand, increasing the sampling time interval (i.e., reducing the sampling frequency) will result in a larger uncertainty. A recent survey of sampling uncertainty for various geophysical parameters is provided by Astin (1997).

Motivated by these earlier studies, therefore, the sampling-related uncertainty σ_E is assumed to be a function of the rainfall rate R, the domain size A, the time integration T, and the sampling time interval Δt according to

$$\sigma_E = f\left(\frac{1}{R}, \frac{1}{A}, \frac{\Delta t}{T}\right). \quad (1)$$

A specific analytical framework for estimation of the sampling uncertainty is developed in section 2. Using a multiyear dataset of continental-scale, radar-based rainfall observations over the United States east of the Rocky Mountains, the sampling-related uncertainty of averages of observations made at regular time intervals is studied in depth (section 3). Irregularities in the space–time sampling pattern (e.g., Salby 1982a,b; Wunsch 1989; Chelton and Schlax 1991; Wu et al. 1995; Zeng and Levy 1995; Negri et al. 2002) and issues of

Corresponding author address: Dr. Matthias Steiner, Department of Civil and Environmental Engineering, Princeton University, Princeton, NJ 08544.
E-mail: msteiner@princeton.edu

rainfall retrieval accuracy (e.g., Wilheit 1988; Bell et al. 1990, 2001; Ha and North 1995) or combination of observations from multiple satellite platforms (e.g., Shin and North 1988; North et al. 1993; Bell and Kundu 1996) are not considered as part of this analysis.

The sampling-related uncertainty is evaluated as a function of typical space and time domains, sampling frequency, and the rainfall intensity. The present analyses go beyond what previous studies have achieved in at least two major ways: 1) an extensive database is explored in depth and 2) two distinctly different approaches of estimating the sampling-related uncertainty are compared. Moreover, an attempt is made to characterize the accuracy of such uncertainty estimates.

This study thus aims at quantifying the uncertainty (often dubbed the *sampling error*) of remotely sensed rainfall estimates based on discrete sampling in space and time. The results will provide guidance for interpretation of rainfall estimates from satellites, such as the Tropical Rainfall Measuring Mission (TRMM) satellite (Simpson et al. 1988, 1996; Kummerow et al. 1998) or the Advanced Microwave Sounding Units (AMSU) flown aboard the current operational National Oceanic and Atmospheric Administration (NOAA) polar-orbiting satellite series (e.g., Kidder et al. 2000; Ferraro et al. 2002), and planning of future satellite missions, such as the Global Precipitation Measurement (GPM) mission.

2. Analysis procedures and data

a. A framework for estimation of sampling uncertainty

There are at least two different statistical approaches to estimating the sampling-related uncertainty of rainfall: parametric methods (with stochastic space–time rainfall model parameters fitted to data) and nonparametric, purely empirical methods (based on subsampling scenarios). These latter methods typically build on *resampling by shifts* techniques based on high-resolution rain gauge and/or radar data (e.g., McConnell and North 1987; Steiner 1996; Li et al. 1996). A mathematical framework is developed here that enables direct comparison of the two approaches.

In the study of sampling uncertainty by Laughlin (1981), a satellite is assumed to make its first observation at $t = 0$, subsequent observations at regular intervals of Δt, and its last observation at $t = T$. The resampling by shifts method of estimating the sampling-related uncertainty assumes instead that the simulated satellite observations begin at an arbitrary time t_0 with $0 \le t_0 < \Delta t$. Laughlin's approach, however, can easily be modified to accommodate arbitrary starting times within the averaging interval $[0, T]$, as summarized below. Except for the starting time, the assumptions are the same as in Laughlin (1981): the satellite sees an area A (all of it) at intervals Δt during a time period T. Sampling begins at starting time t_0, and a total of $n = T/\Delta t$ samples are collected. Regardless of the starting point t_0, the *true* average rainfall is defined to be

$$\overline{R} = \frac{1}{T}\int_0^T R_A(t)\, dt, \tag{2}$$

while the *sample* average, with starting time t_0, is

$$\hat{R}(t_0) = \frac{1}{n}\sum_{k=0}^{n-1} R_A(t_0 + k\Delta t). \tag{3}$$

Here, $R_A(t)$ is the instantaneous rain rate at time t averaged over a grid box with area A. The error in the sample average due to the discrete sampling for a particular starting time t_0 is

$$\varepsilon(t_0) = \hat{R}(t_0) - \overline{R}. \tag{4}$$

The resampling by shifts method (nonparametric approach) obtains an estimate of the mean-squared sampling uncertainty σ_E^2 from the average of $\varepsilon^2(t_0)$ over all possible values of t_0 in the interval $0 \le t_0 < \Delta t$, which may be denoted as

$$\sigma_E^2 = \langle \varepsilon^2(t_0) \rangle_{t_0}. \tag{5}$$

Using the same statistical assumptions as Laughlin (1981), an estimate of (5) for the parametric approach is derived in the appendix, with the result

$$\sigma_E^2 = \langle [\hat{R}(t_0) - \overline{R}]^2 \rangle_{t_0} \approx \sigma_A^2 \frac{\Delta t}{T} c_1\left(\frac{\Delta t}{\tau_A}\right), \tag{6}$$

where

$$c_1(z) = \coth(z/2) - 2/z. \tag{7}$$

Here, σ_A^2 is the variance and τ_A the correlation time (i.e., $1/e$-folding time of the autocorrelation) of the instantaneous area-average rain rate $R_A(t)$. Terms that only become significant for small T are omitted in Eq. (6). Their contributions to the sampling uncertainty estimate are discussed in the appendix. Shin and North (1988), Bell and Kundu (1996, 2000), and Bell et al. (2001) provide additional background for the derivation of Eq. (6). We refer to approximation (6) as the Laughlin–Bell approach.

Equation (6) predicts that σ_E should be approximately linear in Δt for small Δt, because a power series expansion of (6) gives

$$\sigma_E^2 = \sigma_A^2 \left[\frac{(\Delta t)^2}{6\tau_A T} - \frac{(\Delta t)^4}{360\tau_A^3 T} + \cdots \right]. \tag{8}$$

For $T \gg \tau_A$ (typically $\tau_A \sim$ 3–8 h), this is well approximated by

$$\sigma_E \approx \frac{\sigma_A}{\sqrt{6\tau_A}} \frac{\Delta t}{\sqrt{T}}. \tag{9}$$

Because the next order correction term in (8) is fairly small, the linearity between σ_E and Δt may persist over a substantial range of values of Δt. As Δt becomes large

compared with the correlation time τ_A, however, (6) predicts that σ_E should begin to scale more like $\sqrt{\Delta t}$.

It should be noted that this linearity in Δt is a consequence of Laughlin's (1981) assumption that the autocorrelation of the area-average rain rate behaves like an exponential $e^{-\tau/\tau_A}$ for small lags τ. An autocorrelation that did not drop off so quickly for small lags, as $e^{-(\tau/\tau_A)^2}$, for instance, would lead to sampling uncertainty increasing as a higher power of Δt. As we will see later (section 3), the data exhibit an approximately linear dependence on Δt over the sampling frequency range investigated, suggesting that the autocorrelation of $R_A(t)$ may be roughly exponential.

The sampling uncertainty σ_E is predicted by Eq. (6) to be proportional to $T^{-0.5}$. For T small enough, there is the possibility that the terms omitted from (6) might predict deviations from this simple proportionality. As shown in the appendix, however, even for T as small as 1 day the deviations from the inverse square root scaling are small. (See also results discussed in section 3.)

How does σ_E depend on the area A? This is not quite as easy to assess, because the dependence of σ_E on A is governed both by the dependence of σ_A and of τ_A on A. For large A, assuming that the spatial and temporal correlation of rain events decreases rapidly for sufficiently large space and time separations, it is likely that $\sigma_A \sim A^{-0.5}$ and that τ_A may become independent of A; thus, for large space domains σ_E may be proportional to $A^{-0.5}$. For small A, however, this may not generally be the case. In radar data collected during the Global Atmospheric Research Program (GARP) Atlantic Tropical Experiment (GATE; Kuettner et al. 1974), for example, a behavior like $\sigma_A^2 \approx 25A^{-0.33}$ mm^2 h^{-2} and $\tau_A \approx 0.39A^{0.26}$ h is seen (Bell 1987; Bell et al. 1990), where A has units of km^2. The dependence of σ_E on A for small A, if the fits to GATE statistics are to be believed, is thus approximately $\sim A^{-0.3}$ according to (9).

b. Data and analysis procedures

The analyses of the sampling-related uncertainties are based on a multiyear, continental-scale, merged radar data product provided by Weather Services International (WSI) Corporation at a resolution of approximately 2 km in space and 15 min in time. Radar reflectivity of this product comes at 16 discrete levels. For the purpose of our analyses, the radar reflectivity factor Z was converted to rainfall rate R using a hail threshold of 55 dBZ and a gauge-adjusted $Z = 600R^{1.4}$ relationship. A more detailed description and different use of this data product may be found in Carbone et al. (2002). Issues about the radar rainfall estimation are extensively discussed in Steiner et al. (1999) and references therein.

This dataset may not reflect the true rainfall that occurred at any given point in space and time; however, it provides a *most realistic* representation of rain variability over the continental United States east of the Rocky Mountains. The gauge adjustment resulted in essentially unbiased radar rainfall estimates, as shown in Fig. 1. The analyses of the sampling-related uncertainty are thus on good grounds, particularly because they build primarily upon relative comparisons rather than absolute values, as detailed later.

The analyses discussed here are focused on the summer months June 1999 (Fig. 1c), July 2000 (Fig. 1d), August 1997 (Fig. 1e), and September 1998 (Fig. 1f). These months were selected to represent data from various months and years, and to have minimal data gaps (less than 3 rainfall maps missing in total). Data gaps were filled by linear interpolation between time steps for each grid point individually. The present study domain spans approximately 35°–45°N in latitude and 80°–100°W in longitude (Fig. 1a). Roughly speaking, this domain covers the area in between the Rocky Mountains (to the west) and the Appalachian Mountains (to the east), and reaches from Texas (in the south) to the Great Lakes (in the north).

The study area was divided into squared domains with side length L ($L = A^{0.5}$) of 500 km (6 domains), 200 km (48), or 100 km (192), respectively, and rainfall observations were integrated over time periods T of 30 days (1 period), 5 days (6), or 1 day (30) for our analyses. The sampling-related uncertainty was assessed for sampling time intervals Δt of 12, 8, 6, 3, and 1 h, and 15 min (full resolution), respectively. Analyses were carried out for all combinations of domain size, time period, and sampling frequency for all 4 months investigated.

1) Approach based on resampling by shifts

The basic analysis procedure is that of a subsampling exercise to determine how much uncertainty is typically present in rainfall estimates, as a function of the frequency of sampling. The rainfall for a given time period is estimated from samples obtained at regular time intervals, assuming that each sample is representative of what occurred during the unobserved interval around it. All possible sampling scenarios based on the 15-min data and the selected sampling time interval are analyzed (by *shifting* the start time) and comparing the sample average to the rainfall estimate based on using all samples, as outlined in section 2a.

The sampling-related uncertainty σ_E, estimated as the standard deviation of the rainfall estimates obtained by successive shifts of the start time, is expressed relative to the true average rainfall as

$$\frac{\sigma_E}{\overline{R}} = \frac{\sqrt{\mathrm{var}[\varepsilon(t_0)]}}{\overline{R}}, \tag{10}$$

where $\mathrm{var}[\varepsilon(t_0)]$ is the variance of rainfall errors $\varepsilon(t_0)$ as defined in (4), over all possible shifts in the starting time t_0. This variance typically increases with decreasing sampling frequency.

The resampling by shifts procedure has been em-

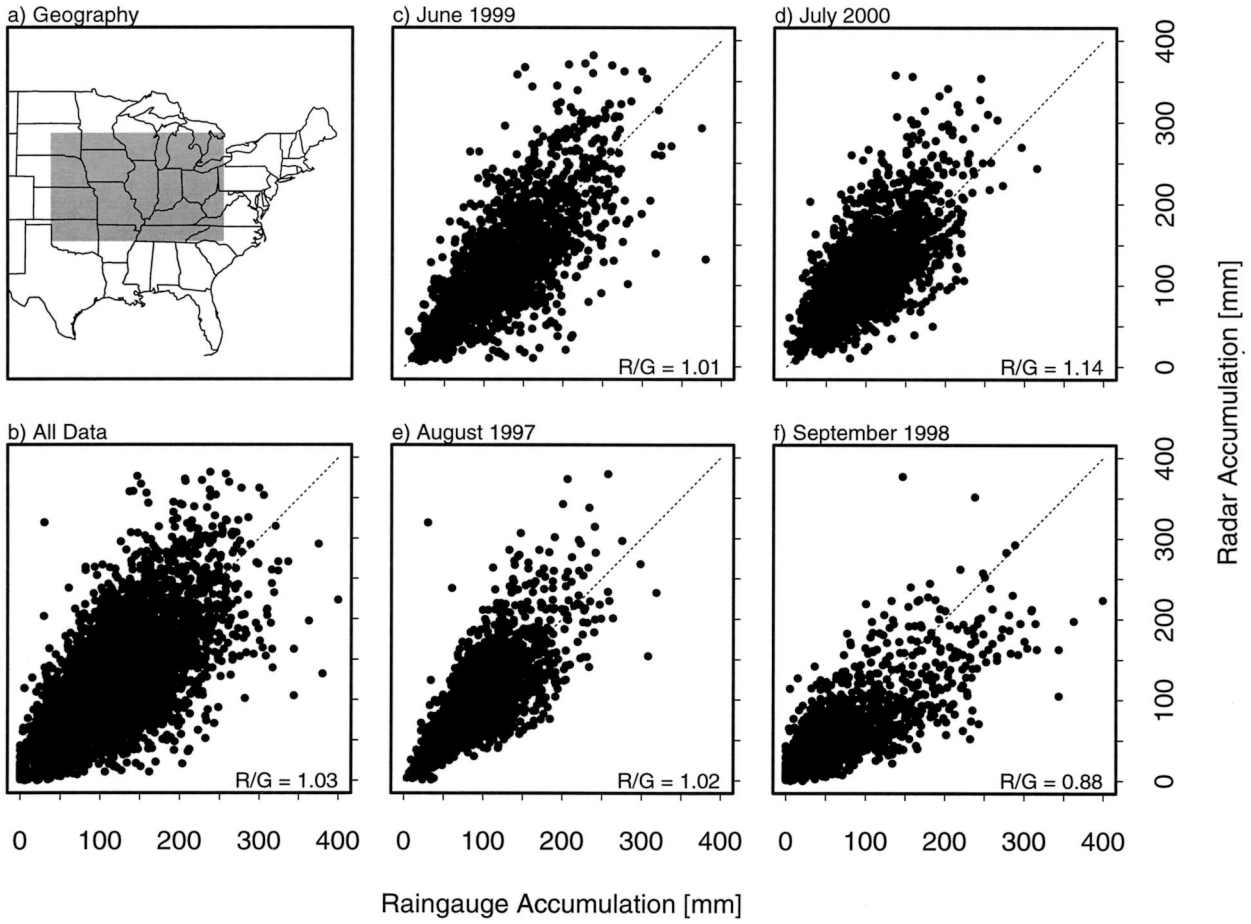

FIG. 1. Geography and radar rainfall calibration. (a) Study domain (shaded in gray) covering the Great Plains of the United States. The approximate boundaries of this domain are 35°–45°N and 80°–100°W. (b) Radar-based vs gauge-accumulated rainfall for all 4 months combined. (c)–(f) Radar vs gauge rainfall for Jun 1999, Jul 2000, Aug 1997, and Sep 1998, respectively. The ratio of mean radar to mean gauge rainfall is indicated in each bottom-right corner.

ployed in numerous studies (e.g., McConnell and North 1987; Steiner et al. 1995; Soman et al. 1995; Steiner 1996; Li et al. 1996). Steiner (1996), for example, used this methodology to estimate the sampling-related uncertainty of surface rainfall based on extensive rain gauge information. Using radar data, these analyses were subsequently expanded by Steiner and Houze (1998) to examine the sampling uncertainty of the entire three-dimensional structure of rainfall.

2) Approach based on Laughlin and Bell

The sampling-related uncertainty is estimated based on the Laughlin–Bell approach according to Eqs. (6) and (7) described in section 2a. The key rainfall parameters needed are the variance σ_A^2 and time correlation τ_A of the area-average rainfall-rate time series $R_A(t)$. As in Eq. (10), the sampling-related uncertainties are expressed relative to the true rain rate as $\sigma_E/\overline{R}$.

Figures 2–4 show the distributions of three key parameters for the 4-month dataset: the space and time domain-average true rain rate $\overline{R}$ (Fig. 2), the variance in time σ_A^2 of the instantaneous area-average rain rates (Fig. 3), and the time correlation τ_A of the instantaneous area-average rain rates (Fig. 4).[1] The number shown in the bottom-right corner of a panel indicates the sample size contained in that distribution. The distributions are normalized using their respective sample size. The maximum value of a given distribution is shown in the upper-right corner of the panel.

The rain-rate distribution significantly widens with decreasing time integration, but also with decreasing domain size (albeit not as quickly), as shown in Fig. 2. This is expected because reduced levels of averaging

[1] The correlation time τ_A of the instantaneous area-average rain rate is determined as the $1/e$-folding time of the autocorrelation. The autocorrelation function is obtained by dividing all covariances by the geometric mean of the corresponding variances. The covariance function is estimated by summing the lagged products and dividing by the length of the time series. The S-PLUS software package was used, which is available from Statistical Sciences, Inc., Seattle, Washington 98109.

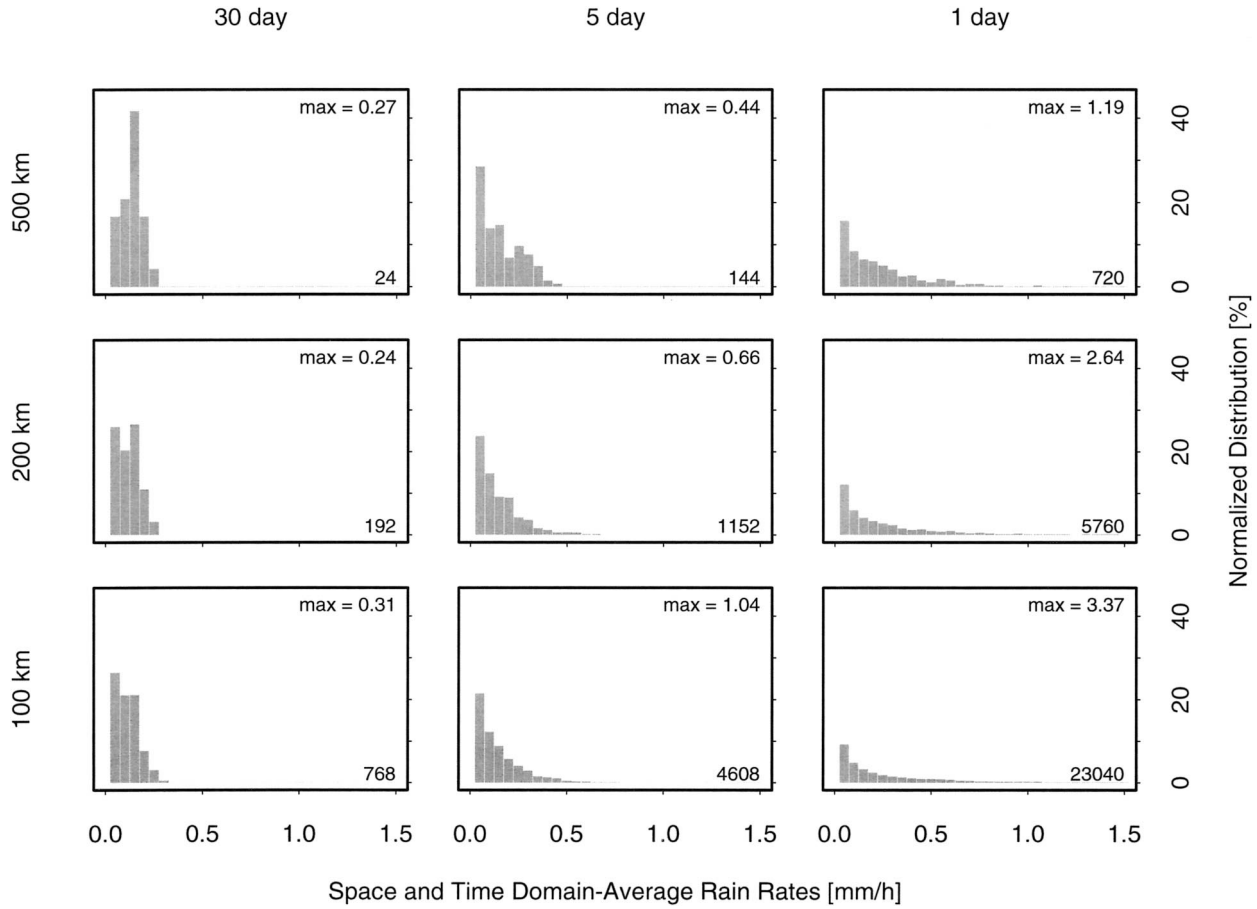

FIG. 2. Distributions of space and time domain-average rain rate $\overline{R}$ based on 4 months of data for three averaging areas and three averaging periods. The sample size, indicated by the number in each bottom-right corner, is used to normalize the respective mean rain-rate distribution. The maximum value of each distribution is shown in the top-right corner.

will retain peak rain-rate values more easily. The maximum space and time domain-average rain rate increases from approximately 0.3 mm h^{-1} for the 500-km and 30-day setting (Fig. 2, top left) to roughly 3.4 mm h^{-1} for the 100-km and 1-day configuration (bottom right). To put this in perspective, a rainfall of 0.3 mm h^{-1} intensity accumulates approximately 7 mm day^{-1} and 220 mm $month^{-1}$. At 3.4 mm h^{-1} more than 80 mm of rain (averaged over a 10 000 km^2 area) are generated in a day. The 4-month dataset thus comprises a representative range of mean rain rates.

The variance σ_A^2 of the area-average rain-rate trace increases rapidly both with decreasing space and time domain, as shown in Fig. 3. The time correlation τ_A of the area-average rain-rate trace, however, exhibits a rather different behavior (Fig. 4). Although the maximum of τ_A appears to be similar for given time periods, independent of the space domain, the bulk of the distribution of correlation times clearly shifts to smaller values with decreasing space and time domains. A bimodal distribution with typical values of $\tau_A \sim 5.5$ and 8.5 h is seen for monthly rainfall on a 500-km domain. Much shorter time correlations (<3 h) are observed for daily rainfall on 100-km domains. The reduction in correlation times evaluated using the 1-day time series may, in part, be due to a bias introduced by the standard estimator of autocovariances.

The coefficient of variation $\sigma_A/\overline{R}$ of the area-average rain rates is directly proportional to the sampling uncertainty σ_E, as can be seen from (9). This rainfall parameter, shown in Fig. 5, will be used later in the discussion of results (section 3c).

3. Results and discussion

a. Characteristics of rainfall sampling uncertainty

The sampling-related uncertainty is estimated for any combination of the various space and time domains, and sampling frequencies explored based on the 4-month dataset. Note that the examined dataset represents the equivalent of 2 yr worth of data for a 500-km domain, 16 yr for a 200-km domain, and 64 yr for a 100-km domain. Moreover, the sampling uncertainty is estimated using two distinctly different approaches, as outlined in section 2b. The results obtained using the re-

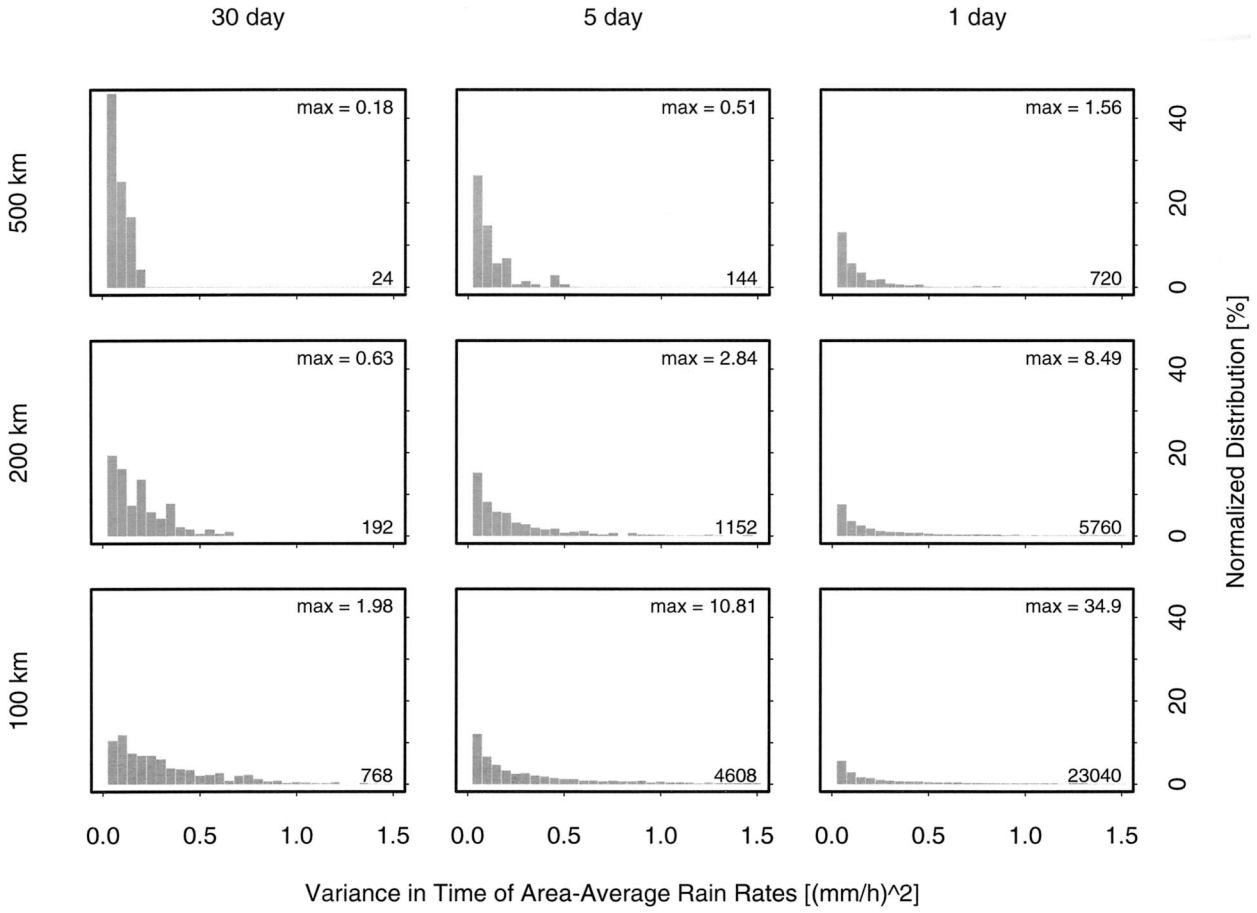

FIG. 3. Distributions of the variance σ_A^2 of the instantaneous area-average rain rate $R_A(t)$ based on 4 months of data. The corner notations are similar to Fig. 2.

sampling by shifts technique are discussed first. The results using the Laughlin–Bell approach will be described in section 3b.

Figure 6 summarizes the results of estimating the sampling uncertainty for the nine possible combinations based on three space (500, 200, and 100 km) and three time (30, 5, and 1 day) domains. In addition, within each panel the results for five sampling time intervals (1, 3, 6, 8, and 12 h) are shown. The sampling uncertainty distributions are represented by their full range of values (bold solid line), the center 50% of values (outlined box), and the distribution median (bold dot). The results shown in Fig. 6 are limited to space- and time-domain-average rain rates $\overline{R} \sim 0.1$ mm h^{-1} (i.e., $0.075 < \overline{R} \leq 0.125$ mm h^{-1}). Results for other mean rain rates are presented later. The corresponding sample size (identical for all sampling frequencies) is indicated by the number in the bottom-right corner of each panel. The dotted line (and shaded area) indicates sampling uncertainty estimates (and range of uncertainty) based on a fitted scaling law to the data, as will be discussed later as well.

The sampling-related uncertainty clearly scales with space and time domain, and with sampling frequency, as can be seen from Fig. 6. The larger the space and time domain the smaller is the sampling uncertainty. Similarly, the higher the sampling frequency (i.e., smaller sampling time interval) the smaller is the related uncertainty. However, even for a narrow rain-rate range of $0.075 < \overline{R} \leq 0.125$ (nominal $\overline{R} \sim 0.1$ mm h^{-1}), a very significant range of sampling uncertainty is observed. This range of sampling uncertainty is a reflection of the great variability of rainfall in space and time. For example, for a TRMM-like sampling[2] of $\Delta t \sim 12$ h, the median of the distribution of sampling uncertainty for daily rainfall on a 100-km domain (bottom right of Fig. 6) is 154%, yet the center 50% of the distribution spans from 116% to 196% (extreme values of sampling uncertainty are found as low as 40% and as high as 460%). For a GPM-like sampling ($\Delta t \sim 3$ h), this sampling uncertainty drastically reduces to 43% (median), with half the estimates falling within the range of 26%–67%.

[2] Note that at the equator the true TRMM sampling is closer to $\Delta t \sim 24$ h. For simplicity, however, variable sampling intervals as a function of latitude are not considered in this study.

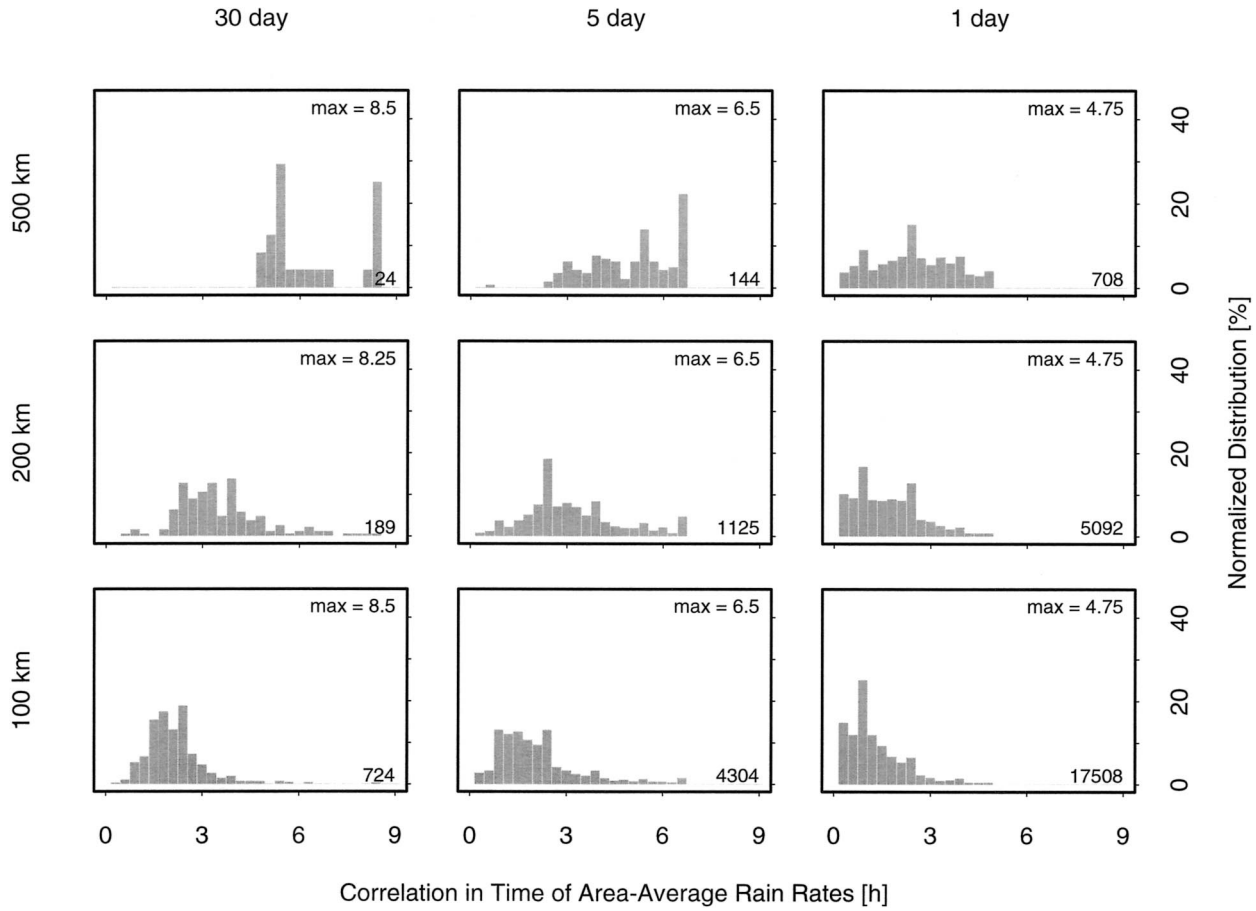

FIG. 4. Distributions of the time correlation τ_A of the instantaneous area-average rain rate $R_A(t)$ based on 4 months of data. The corner notations are similar to Fig. 2.

The sampling-related uncertainties for monthly rainfall on a 500-km domain (top-left of Fig. 6), as observed by a TRMM-like satellite platform, show a median value of 17%, with the center 50% of values falling between 8% and 20%.

Similarly to Fig. 6, the sampling-related uncertainty may be shown for any mean rain rate. Rain rates of 0.5, 1.0, and 1.5 mm h^{-1} are selected to highlight the scaling of sampling uncertainty with rain rate in Fig. 7; however, results are shown for 1-day periods only. No samples exhibited mean rain rates of 1 and 1.5 mm h^{-1}, respectively, for daily rainfall on 500-km domains. Similarly, there were no samples with mean rain rates of 1.5 mm h^{-1} for daily rainfall on 200-km domains. Nonetheless, the scaling of sampling uncertainty with domain size can be seen for all rain rates, and by comparing Figs. 6 and 7 a scaling with rain rate becomes apparent.

In order to quantify the scaling of sampling uncertainty with space and time domain size, sampling frequency, and mean rain rate, the distribution medians were determined for all 45 combinations of space (3 options) and time (3) domains, and sampling frequencies (5). The median was selected rather than the mean because of its much reduced sensitivity to extreme values (outliers). Moreover, this was done for the rain-rate range of $0 < \overline{R} \leq 3.5$ mm h^{-1} in steps of 0.05 mm h^{-1} (70 intervals). The resulting large ensemble of distribution medians was then used to fit the coefficients *a*, *b*, *c*, *d*, and *e* of the following, empirically guided, simple sampling uncertainty scaling law:

$$\frac{\sigma_E}{\overline{R}}100\% = a\left(\frac{R_0}{\overline{R}}\right)^b\left(\frac{L_0}{L}\right)^c\left(\frac{T_0}{T}\right)^d\left(\frac{\Delta t}{\Delta t_0}\right)^e, \qquad (11)$$

by minimizing the root-mean-square (rms) difference between the predicted uncertainty (11) and the corresponding median value, using $R_0 = 1.0$ mm h^{-1}, $L_0 = 500$ km, $T_0 = 30$ day, and $\Delta t_0 = 1$ h, respectively.[3] In addition, sensitivity tests were performed to assess the robustness of the coefficient values (Table 1). In particular, we assessed the variability of the coefficients

[3] The multiplicative factor *a* was adjusted by means of removing the mean difference (bias), while the coefficients *b*, *c*, *d*, and *e* were determined iteratively (in steps of 0.05) to find the minimum rms difference.

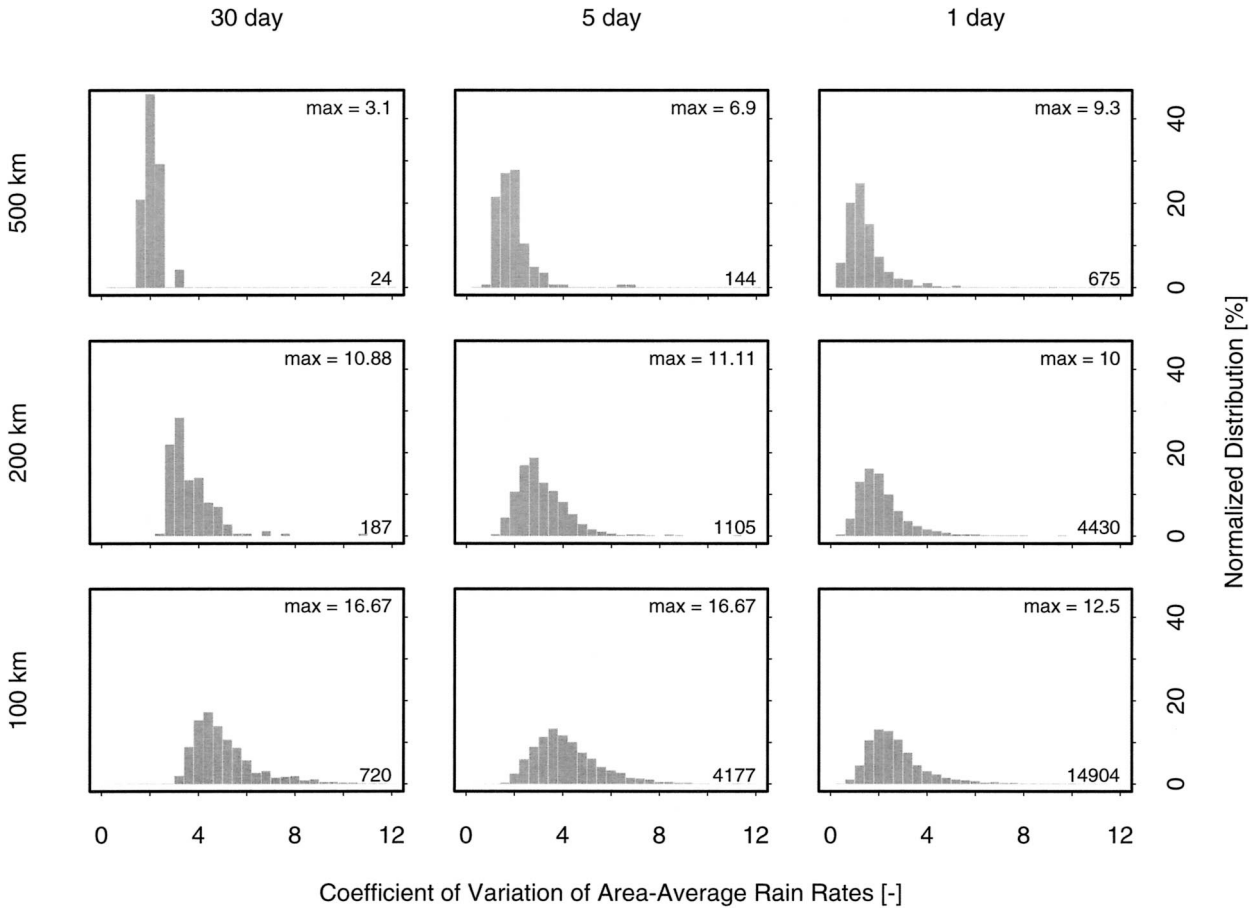

FIG. 5. Distributions of the coefficient of variation $\sigma_A/\overline{R}$ of the instantaneous area-average rain rate $R_A(t)$ based on 4 months of data. The corner notations are similar to Fig. 2.

from month to month, and also used only medians that were based on distributions containing minimally 1, 5, 10, or 15 samples. By increasing the minimum number of samples required in a given distribution, the respective median values are thought to become more representative and thus are given priority in the fitting procedure.

Based on the results summarized in Table 1, we selected $a = 0.80$, $b = 0.20$, $c = 0.70$, $d = 0.35$, and $e = 1.05$ as the ''best fit'' coefficients of (11). These coefficients exhibit some variability from month to month and depend on the underlying data constraints; however, overall they appear to be rather robust estimates. The exponents (i.e., coefficients *b*, *c*, *d*, and *e*) may be uncertain at the 10% level and the overall prediction of sampling uncertainty at the 25% level, based on the results compiled in Table 1 and experimentation with weighted fitting procedures in logarithmic space (not shown).

Equation (11), using the fitted coefficients, displays a scaling of sampling-related uncertainty of rainfall estimates that is pretty much linear in sampling time interval Δt ($e = 1.05$)—at least for the range $0 < \Delta t \leq$ 12 h investigated (see Figs. 6 and 7)—similar to the results obtained by Steiner (1996) or Li et al. (1996), and as predicted by Eq. (9). A linear scaling in Δt suggests that the autocorrelation of the area-average rain rate should decrease roughly exponentially, as originally assumed by Laughlin (1981). This linearity predicted for small Δt, however, depends only on the small-lag behavior of the autocorrelation, and does not contradict potentially different behavior for longer time lags, as is sometimes observed. For example, Rodriguez-Iturbe et al. (1998) provide evidence that rainfall observations appear to have a long-range memory, which suggests that the scaling with sampling time interval might change for larger Δt. In fact, Weng et al. (1994) show that an approximate linearity in scaling of sampling uncertainty for $\Delta t < 12$ h starts to break down for $\Delta t >$ 12 h. The scaling of sampling uncertainty with time domain *T* ($d = 0.35$) is close to (albeit not quite) the inverse square root behavior advocated by (9). The scaling with space domain size *L* ($c = 0.70$) is very similar to what would be predicted from GATE I rainfall data, as discussed in section 2a.

Figure 8 highlights the scaling of sampling uncer-

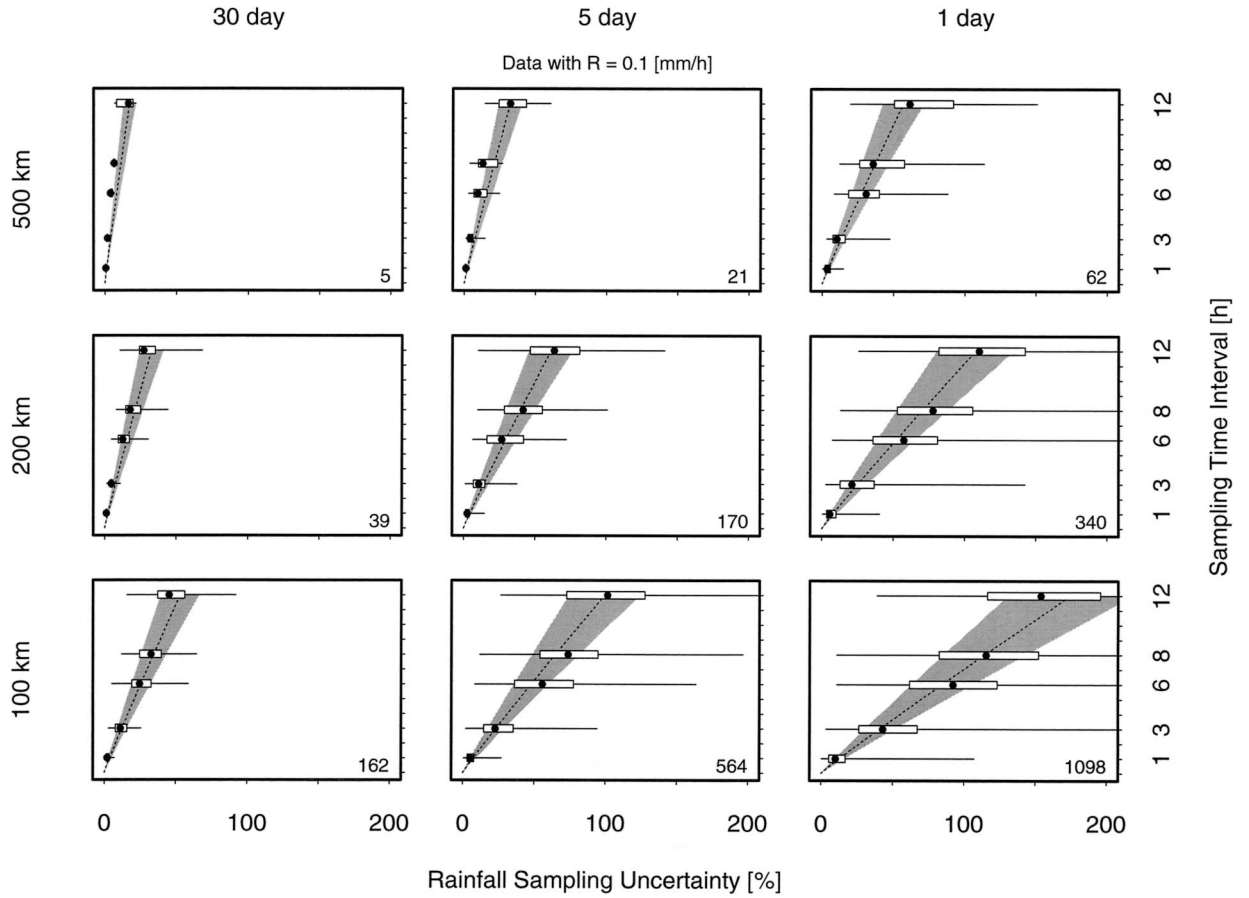

FIG. 6. Distributions of the sampling-related uncertainty (determined by the resampling by shifts approach) as a function of space and time domain, and sampling frequency. Shown are the results for a space and time domain-average rain rate of $\overline{R} \sim 0.1$ mm h^{-1} based on the 4-month dataset. The full range of each distribution is shown by the solid line, the outlined box indicates the center 50% of the values, and the bold dot marks the distribution median. The sample size for each distribution (identical for all sampling frequencies shown within a panel) is indicated by the number in the bottom-right corner. The dotted line is based on the fitted scaling law (11) characterizing the sampling-related uncertainty as a function of space and time domain, and sampling frequency, with $\overline{R} = 0.1$ mm h^{-1}. The surrounding shaded area marks the predicted sampling uncertainty ±25% of its value.

tainty with mean rain rate $\overline{R}(b = 0.20)$, showing a clear departure from the inverse square root behavior suggested by simple models (e.g., Bell and Kundu 2000). The scaling of sampling uncertainty as $\overline{R}^{-0.5}$ is born out of the assumption that variations in total rainfall within an area would primarily be due to variations in the number of independently evolving precipitation systems present rather than variations in the intensity of the individual system. If domains with more rain tend also to have larger spatial extent of rainy areas and/or more intense rain, the $\overline{R}^{-0.5}$ dependence may be altered. Apparently the previous assumptions leading to a $\overline{R}^{-0.5}$ behavior are not applicable here.

The shaded areas in Figs. 6, 7, and 8 outline the range of 0.75–1.25 times the sampling uncertainty estimated by (11) using the median-fitted coefficients (dotted lines). This uncertainty range roughly approximates the center 50% of the sampling uncertainties estimated by the resampling by shifts method.

How well does the scaling law (11) based on the fitted coefficients gauge the sampling-related uncertainty using all 4 months' worth of data? The visual impression obtained from Figs. 6, 7, and 8 suggests that the simple scaling law (11) predicts the sampling uncertainty as a function of space and time domain, sampling frequency, and mean rain rate rather well. A closer inspection though, reveals deviations from the approximate linear scaling in Δt. For example, a scaling with sampling time interval of $\Delta t^{e>1}$ is hinted for 500-km domains, while a scaling more like $\Delta t^{e<1}$ is observed for 100-km domains. These nuances become most visible for sampling time intervals of $\Delta t > 8$ h. Recall Fig. 4 that displayed $\tau_A < 3$ h for 100-km domains, which is significantly smaller than the sampling time interval, consistent with the discussion in section 2a.

Tables 2 and 3 compile the actual mean and rms differences (in %) between sampling uncertainties estimated by the resampling by shifts method and predicted by the median-fitted scaling law (11). The mean differences (Table 2) are typically small (a few percent

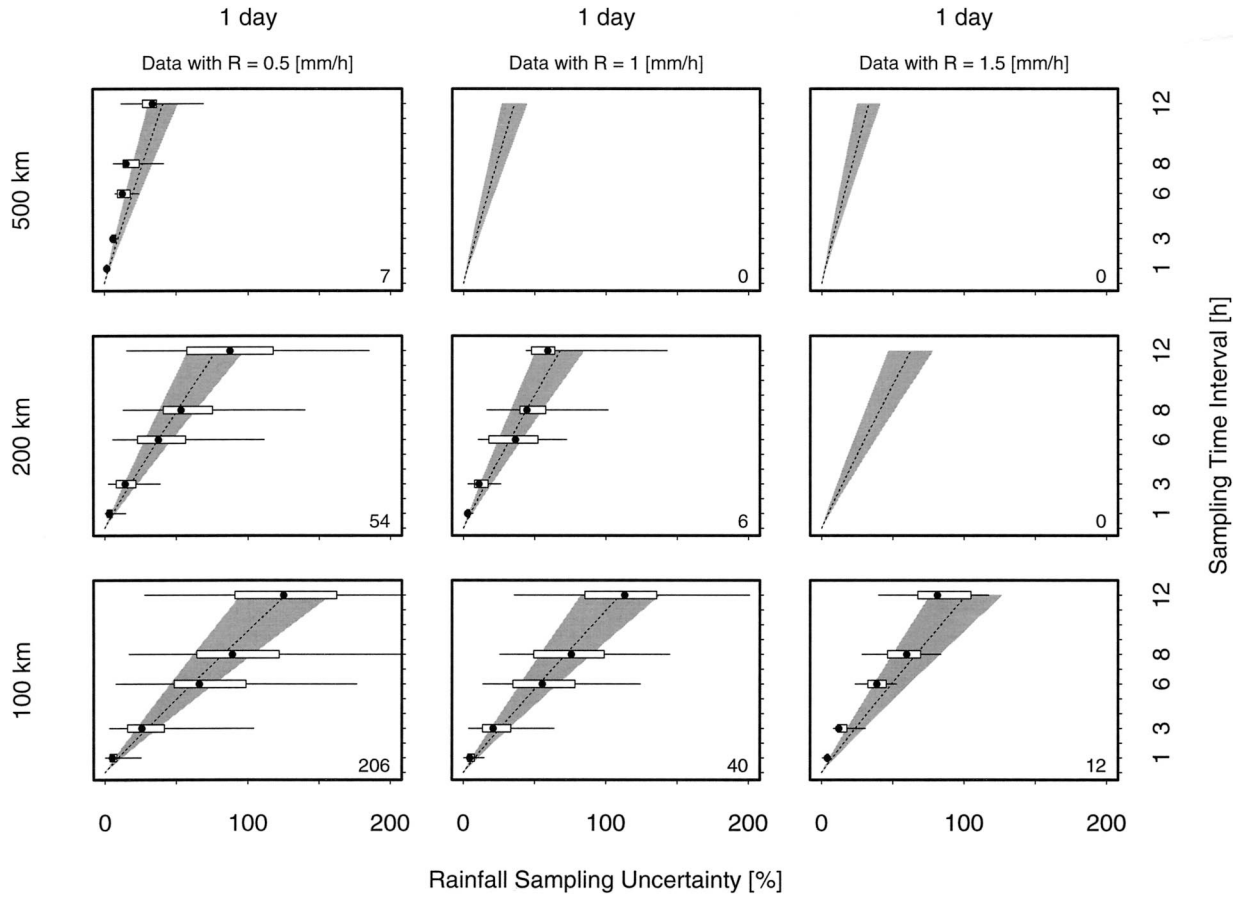

FIG. 7. Distributions of the sampling-related uncertainty (determined by the resampling by shifts approach) as a function of space and time domain, and sampling frequency, similar to Fig. 6. Shown are the results for 1-day rainfall only, but for increasing mean rain rates of (left) 0.5, (middle) 1.0, and (right) 1.5 mm h^{-1}.

TABLE 1. Results of sensitivity analyses for fitting scaling law coefficients to Eq. (11). See text for details.

Data	Medians	Samples	*a*	*b*	*c*	*d*	*e*	Rms
Jun 1999	All	675	0.69	0.20	0.70	0.40	1.05	10.83%
	Min 5 values	420	0.80	0.15	0.65	0.40	1.05	8.96%
	Min 10 values	315	1.01	0.10	0.65	0.35	1.05	7.95%
	Min 15 values	255	1.13	0.10	0.65	0.35	1.00	7.83%
Jul 2000	All	645	0.74	0.25	0.70	0.35	1.05	9.73%
	Min 5 values	425	0.82	0.20	0.70	0.35	1.05	8.23%
	Min 10 values	310	1.05	0.15	0.65	0.35	1.00	8.06%
	Min 15 values	250	1.07	0.15	0.65	0.35	1.00	7.16%
Aug 1997	All	755	0.80	0.15	0.70	0.35	1.05	11.46%
	Min 5 values	365	0.75	0.20	0.70	0.35	1.05	8.07%
	Min 10 values	270	0.80	0.20	0.65	0.35	1.05	7.25%
	Min 15 values	210	0.81	0.20	0.65	0.35	1.05	6.83%
Sep 1998	All	535	0.64	0.25	0.75	0.40	1.00	14.75%
	Min 5 values	275	0.97	0.20	0.65	0.35	1.00	10.71%
	Min 10 values	210	1.25	0.15	0.65	0.30	1.00	7.97%
	Min 15 values	165	1.28	0.15	0.65	0.30	1.00	7.75%
All 4 months	All	845	0.64	0.20	0.75	0.35	1.10	9.22%
	Min 5 values	565	0.70	0.20	0.70	0.35	1.10	7.03%
	Min 10 values	480	0.79	0.20	0.70	0.35	1.05	6.84%
	Min 15 values	410	0.80	0.20	0.70	0.35	1.05	6.76%

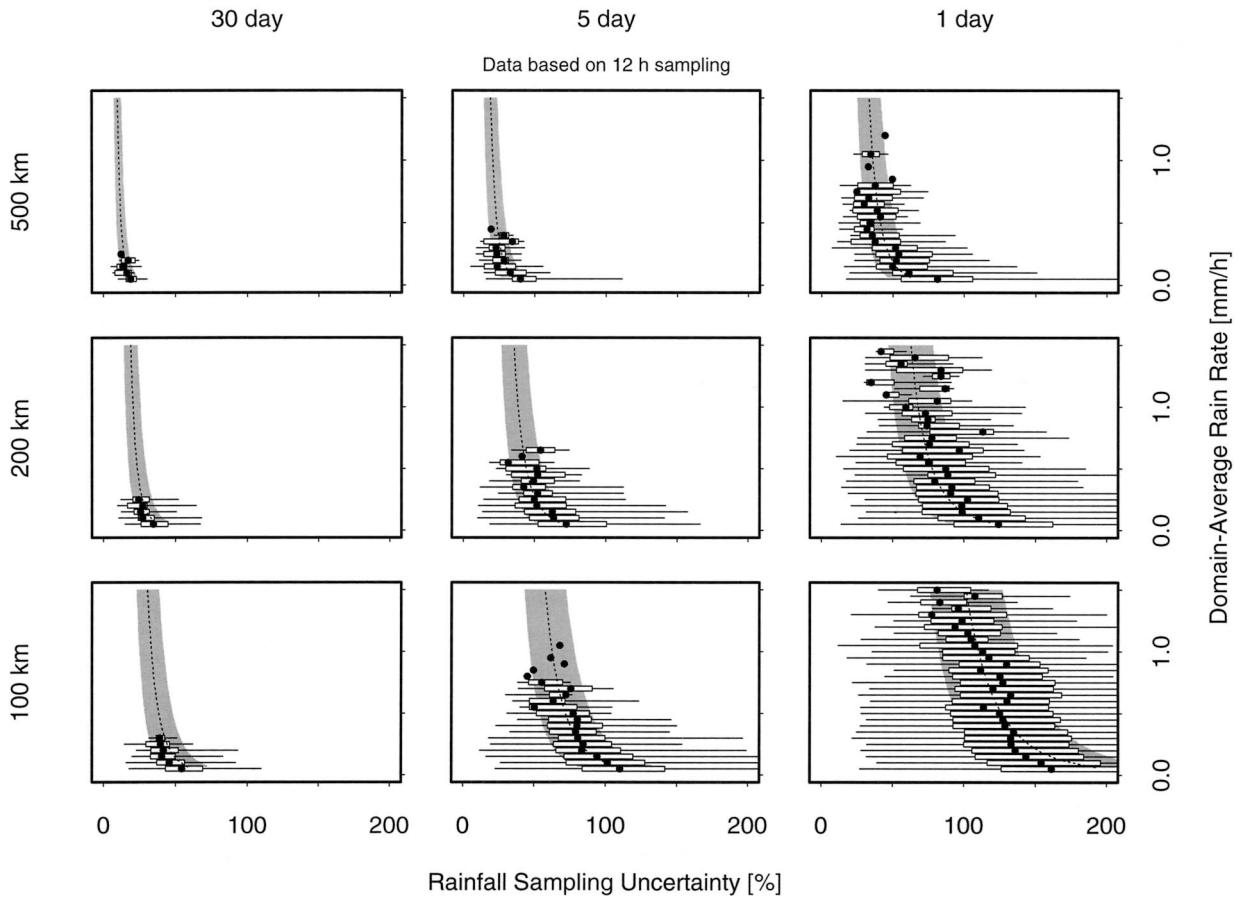

FIG. 8. Distributions of the sampling-related uncertainty (determined by the resampling by shifts approach) as a function of space and time domain, and domain-average rain rate in intervals of 0.05 mm h^{-1}, as used for the fitting of Eq. (11). Results are shown for a sampling time interval of 12 h. The lines, outlined boxes, and shaded areas are similar to Figs. 6 and 7.

TABLE 2. Mean difference between sampling uncertainties estimated by the resampling by shifts approach minus the fitted scaling law (11) using the coefficients $a = 0.80$, $b = 0.20$, $c = 0.70$, $d = 0.35$, and $e = 1.05$. The numbers are based on the results displayed in Figs. 6 and 7.

$\bar{R}$ (mm h^{-1})	T (day)	L (km)	$\Delta t = 1$ h	$\Delta t = 3$ h	$\Delta t = 6$ h	$\Delta t = 8$ h	$\Delta t = 12$ h
0.1	30	500	−0.7%	−2.2%	−3.8%	−5.2%	−2.7%
		200	−1.1%	−2.6%	−2.3%	−0.8%	−3.0%
		100	−1.5%	−0.3%	0.9%	−1.4%	−5.3%
	5	500	−1.1%	−2.5%	−4.3%	−5.4%	0.6%
		200	−1.4%	−2.5%	0.6%	2.9%	4.1%
		100	−1.4%	3.0%	10.5%	10.5%	2.9%
	1	500	−0.2%	−0.2%	2.7%	4.8%	11.9%
		200	−0.2%	2.8%	11.0%	12.9%	9.2%
		100	0.4%	8.8%	11.8%	6.1%	−15.9%
0.5	1	500	−1.4%	−2.9%	−5.7%	−7.1%	−6.8%
		200	−1.8%	−1.8%	4.2%	8.5%	13.2%
		100	−2.8%	2.6%	11.5%	11.5%	2.2%
1.0	1	500	—	—	—	—	—
		200	−1.5%	−2.9%	4.8%	7.0%	1.4%
		100	−2.5%	−0.1%	5.1%	6.2%	2.2%
1.5	1	500	—	—	—	—	—
		200	—	—	—	—	—
		100	−3.4%	−8.4%	−10.6%	−9.4%	−19.2%

TABLE 3. Rms difference between sampling uncertainties estimated by the resampling by shifts approach and the fitted scaling law (11) using the coefficients $a = 0.80$, $b = 0.20$, $c = 0.70$, $d = 0.35$, and $e = 1.05$. The numbers are based on the results displayed in Figs. 6 and 7.

$\bar{R}$ (mm h^{-1})	T (day)	L (km)	$\Delta t = 1$ h	$\Delta t = 3$ h	$\Delta t = 6$ h	$\Delta t = 8$ h	$\Delta t = 12$ h
0.1	30	500	0.8%	2.5%	4.5%	5.9%	7.6%
		200	1.3%	3.5%	6.3%	8.7%	11.8%
		100	1.9%	5.3%	11.1%	11.6%	15.7%
	5	500	1.4%	4.1%	7.8%	9.1%	13.3%
		200	2.6%	7.2%	16.5%	19.9%	27.1%
		100	4.1%	15.5%	29.9%	32.8%	39.5%
	1	500	2.8%	8.3%	15.6%	21.3%	30.2%
		200	6.4%	21.8%	38.0%	43.6%	49.9%
		100	11.7%	32.8%	46.8%	51.6%	62.1%
0.5	1	500	1.7%	3.7%	8.7%	14.6%	19.0%
		200	3.3%	10.3%	24.6%	30.8%	40.1%
		100	5.2%	20.9%	37.5%	42.2%	47.3%
1.0	1	500	—	—	—	—	—
		200	2.5%	9.0%	25.0%	29.6%	37.0%
		100	4.2%	15.4%	29.6%	33.4%	41.0%
1.5	1	500	—	—	—	—	—
		200	—	—	—	—	—
		100	3.9%	11.4%	14.4%	20.7%	33.7%

only); mean differences of 10% or larger are found for $\Delta t \geq 6$ h, but compared to the values of the corresponding distribution median (Figs. 6 and 7) these differences are mostly still relatively small. The rms differences (Table 3), in contrast, show magnitudes comparable to the median values for most space and time domains and sampling time intervals of $\Delta t \leq 6$ h; only lower sampling frequencies reduce the rms differences to a fraction of the respective median values.

These results underline the basic difficulties in estimating sampling-related uncertainties for real rainfall situations. In light of the previous discussion, and because the estimation methods applied are statistical in nature, the derived sampling uncertainties should be expressed in *probabilistic* terms. For example, based on the 4 months' worth of data analyses, there is a 50% chance that the *true* (yet unknown) sampling uncertainty falls within the range of 0.75–1.25 times the sampling uncertainty predicted by the median-fitted simple scaling law (11).

Moreover, in the ''real world,'' attaching a sampling uncertainty to satellite rainfall averages is based on the sample averages themselves, because the underlying true rainfall is unknown. This, of course, introduces additional uncertainty that needs to be quantified. Facing this problem, however, is beyond the scope of the present study.

b. Comparison of two approaches

It is instructive to compare sampling uncertainties that are estimated based on approaches other than the one described in the previous section. The observed differences will highlight a sensitivity of the results to the method applied in obtaining them. Here, sampling uncertainties estimated by the resampling by shifts technique (nonparametric approach) are contrasted with results obtained by the (parametric) Laughlin–Bell approach based on approximation (6). Figures 9 and 10 show this comparison for the same data as displayed in Figs. 6 and 7, respectively. For clarity of the figures, however, the data are shown in a slightly different way: there are fifteen panels for all combinations of time periods and sampling frequency, and the results are distinguished in colors by domain size (500 km in red, 200 km in green, and 100 km in blue).

The encouraging outcome of this comparison is that the sampling uncertainties estimated by both the nonparametric and parametric statistical approaches agree rather well, independent of the space and time domain, and sampling frequency, as demonstrated by Figs. 9 and 10. A closer look, however, reveals that there is significant variability (and potentially some minor trends) among the results that has to be attributed to differences in the way the sampling uncertainty is estimated. Some, but not all, differences can be explained by the correction terms omitted from (6), as is shown in the appendix. Interpreting these nuances, however, is not straightforward and requires further evaluation.

Tables 4 and 5 list the actual mean and rms differences of the data displayed in Figs. 9 and 10 to provide some quantitative information about the comparison. The mean difference (Table 4) between the resampling by shifts and the Laughlin–Bell approaches typically amounts to a few percent only (the maximum difference is 12.4%). Most of the time the Laughlin–Bell approach tends to predict sampling uncertainties that on average are slightly larger than those obtained by the resampling by shifts method. This may not fully concur though with the visual impression obtained from Figs. 9 and 10. The mean difference values listed in Table 4 may be influenced by the large number of samples within the range

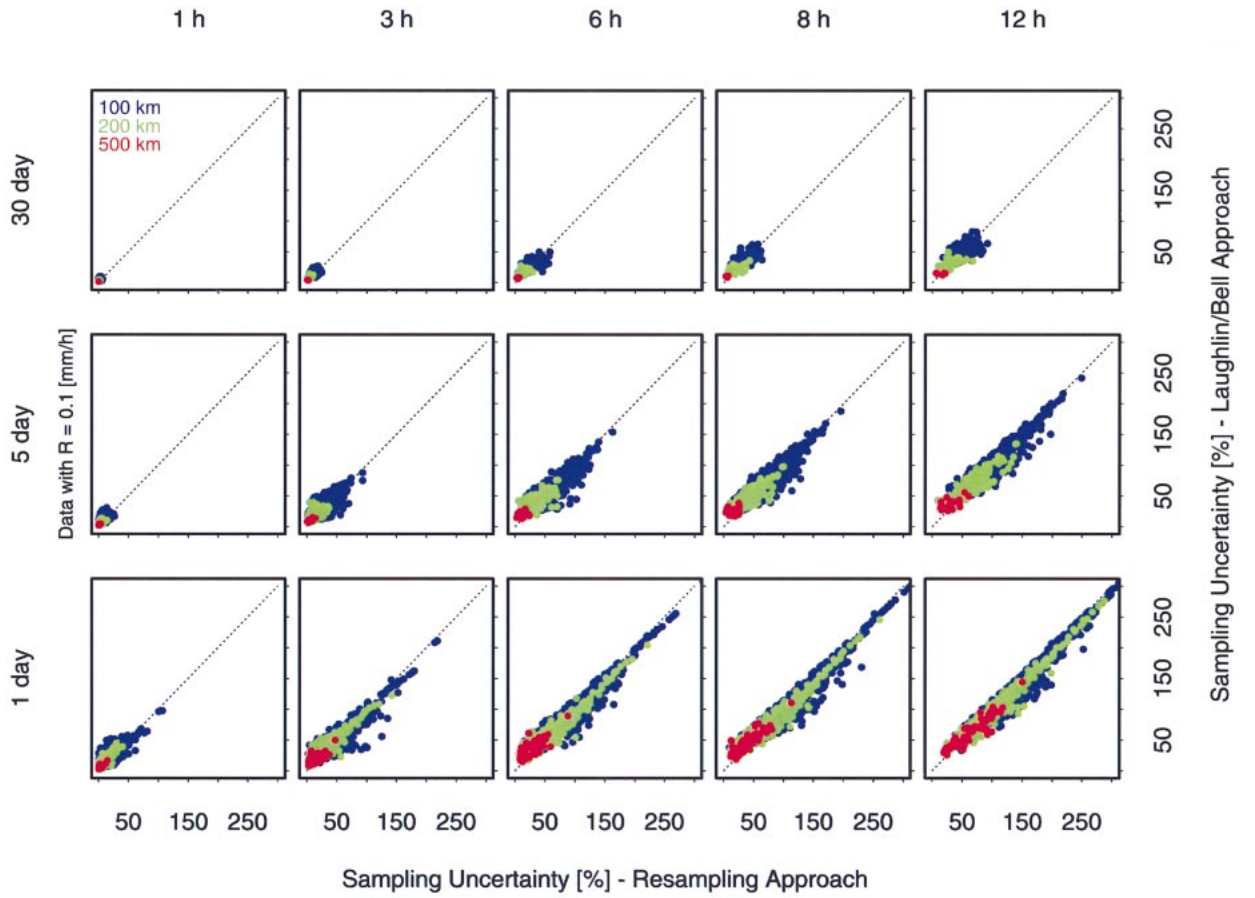

FIG. 9. Comparison of sampling uncertainty estimated by the Laughlin–Bell approximation (6) vs the resampling by shifts estimates for the various explored space and time domains, and sampling frequencies. Shown are the results for a space and time domain-average rain rate of $\overline{R} \sim 0.1$ mm h^{-1} based on the 4-month dataset. The results for the three space domains are shown in different colors (500 km in red, 200 km in green, and 100 km in blue). The dotted line indicates 1:1 correspondence.

of sampling uncertainties smaller than 100%, where the Laughlin–Bell approximation tends toward larger uncertainty estimates than the resampling by shifts approach. For larger sampling uncertainty estimates, the nonparametric and parametric methods yield very similar results—although there is a slight tendency for the resampling by shifts values to exceed the Laughlin–Bell estimates. The rms differences (Table 5) vary between approximately 1% and 17%. Moreover, the rms differences appear to scale with space and time domain size, sampling frequency, and mean rain rate, similar to the estimated sampling uncertainties. For daily rainfall on a 100-km domain observed by a GPM-like sampling ($\Delta t \sim 3$ h), the rms difference between sampling uncertainties estimated by the resampling by shifts and Laughlin–Bell approach is about 12%–13%, which is significantly less than the sampling uncertainty itself (see Figs. 9 and 10) for mean rain rates of 1.0 mm h^{-1} or less. For sampling time intervals $\Delta t \sim 1$ h, the rms differences are of the same magnitude as the median values of sampling uncertainty (Figs. 6 and 7). Especially for longer sampling time intervals, however, the rms differences tend to be a fraction of the sampling uncertainty only. For a TRMM-like sampling ($\Delta t \sim 12$ h), the rms differences are small compared to the value of the sampling uncertainty for all space and time domains examined.

The rms difference between sampling uncertainties estimated by the resampling by shifts method and the Laughlin–Bell approach, as shown in Table 5, is of comparable magnitude or smaller (particularly for $\Delta t \geq 3$ h) than the rms difference between uncertainties estimated by the resampling by shifts method and those predicted by the median-fitted simple scaling law (11), compiled in Table 3. The largest differences occur for infrequent sampling ($\Delta t > 3$ h) of small mean rain rates on smaller domains ($\leq$200 km), where the data-based uncertainty estimates agree more closely with each other than to the uncertainties gauged by the simple scaling law (11).

c. Discussion

There are numerous studies of sampling uncertainty assessments for satellite-based rainfall estimates re-

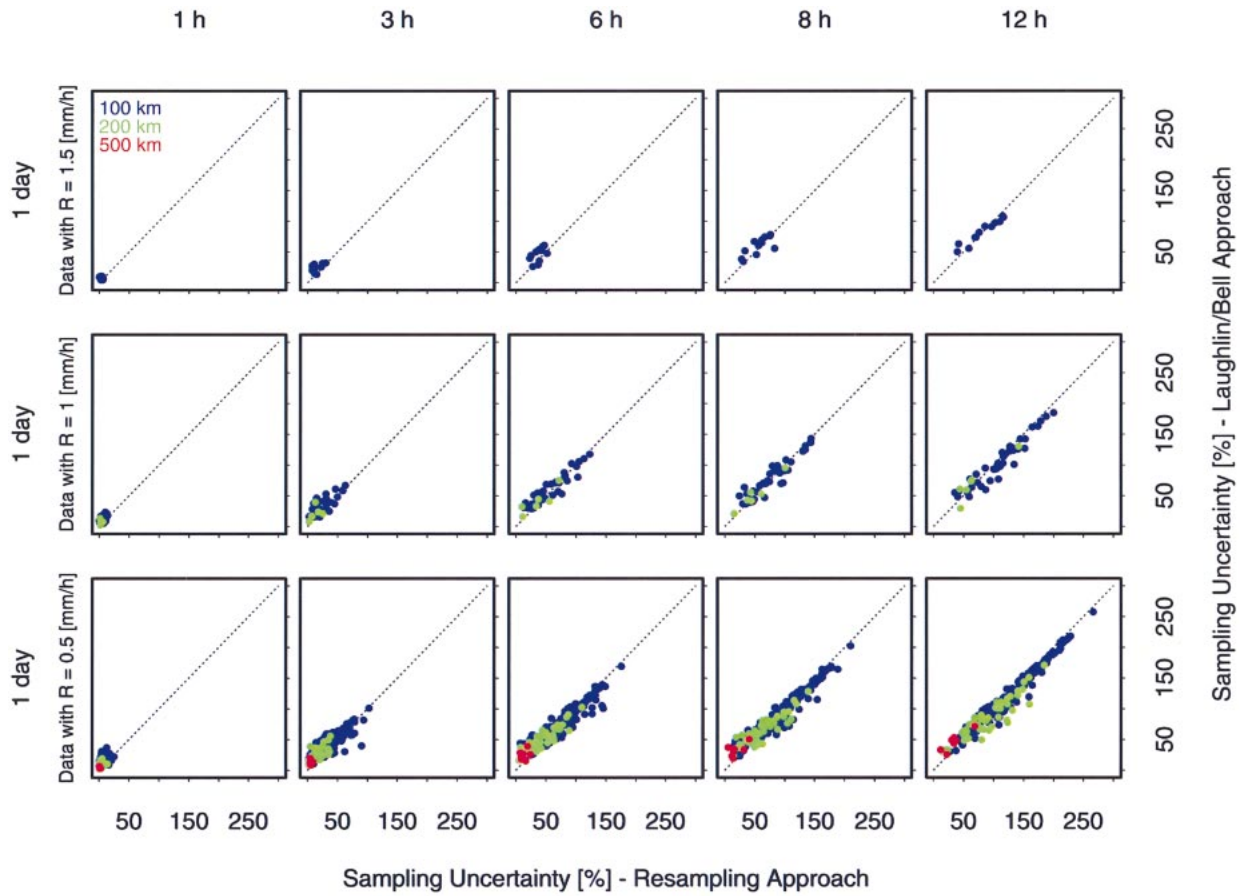

FIG. 10. Comparison of sampling uncertainty estimated by the Laughlin–Bell approximation (6) vs the resampling by shifts estimates for the various explored space and time domains, and sampling frequencies, similar to Fig. 9. Shown are the results for 1-day rainfall only, but for increasing mean rain rates of (bottom) 0.5, (middle) 1.0, and (top) 1.5 mm h^{-1}.

TABLE 4. Mean difference between sampling uncertainties estimated by the resampling by shifts method minus the Laughlin–Bell approach. The numbers are based on the results displayed in Figs. 9 and 10.

$\bar{R}$ (mm h^{-1})	T (day)	L (km)	Δt = 1 h	Δt = 3 h	Δt = 6 h	Δt = 8 h	Δt = 12 h
0.1	30	500	−0.7%	−1.8%	−2.9%	−3.7%	0.2%
		200	−1.5%	−3.5%	−3.2%	−1.2%	−1.4%
		100	−2.5%	−2.5%	−1.1%	−2.0%	−0.6%
	5	500	−2.0%	−4.6%	−7.7%	−9.4%	−3.8%
		200	−3.1%	−6.8%	−6.0%	−4.1%	−1.2%
		100	−4.9%	−5.2%	−0.2%	1.0%	1.3%
	1	500	−2.3%	−5.6%	−5.8%	−4.4%	3.9%
		200	−4.3%	−7.0%	−1.5%	1.8%	6.9%
		100	−5.4%	−2.7%	3.5%	5.8%	8.6%
0.5	1	500	−2.6%	−5.9%	−10.4%	−12.4%	−11.5%
		200	−4.5%	−8.6%	−5.8%	−1.5%	7.3%
		100	−7.1%	−7.5%	−0.2%	2.8%	6.5%
1.0	1	500	—	—	—	—	—
		200	−3.5%	−7.9%	−2.3%	0.0%	−2.0%
		100	−5.6%	−7.3%	−3.0%	0.6%	7.5%
1.5	1	500	—	—	—	—	—
		200	—	—	—	—	—
		100	−4.0%	−8.8%	−7.7%	−2.3%	0.3%

TABLE 5. Rms difference between sampling uncertainties estimated by the resampling by shifts and Laughlin–Bell approaches. The numbers are based on the results displayed in Figs. 9 and 10.

$\overline{R}$ (mm h^{-1})	T (day)	L (km)	Δt = 1 h	Δt = 3 h	Δt = 6 h	Δt = 8 h	Δt = 12 h
0.1	30	500	0.8%	2.3%	3.5%	4.4%	6.9%
		200	1.8%	4.2%	6.7%	8.0%	10.7%
		100	3.0%	5.1%	9.3%	9.7%	12.4%
	5	500	2.2%	5.3%	10.1%	12.7%	12.0%
		200	3.9%	9.8%	12.8%	11.4%	13.1%
		100	6.4%	11.6%	13.2%	13.1%	13.5%
	1	500	3.2%	8.8%	11.6%	10.9%	12.2%
		200	6.3%	12.1%	11.8%	11.6%	12.2%
		100	9.1%	12.5%	12.2%	12.8%	13.3%
0.5	1	500	3.3%	7.8%	14.1%	16.5%	14.6%
		200	5.6%	11.8%	12.4%	12.7%	17.1%
		100	9.1%	13.7%	12.3%	11.8%	11.4%
1.0	1	500	—	—	—	—	—
		200	5.7%	13.2%	12.5%	7.9%	13.6%
		100	7.0%	12.6%	11.3%	11.7%	14.3%
1.5	1	500	—	—	—	—	—
		200	—	—	—	—	—
		100	5.2%	11.8%	12.7%	12.2%	9.7%

ported in the literature. Most of these are (a) based on rather limited data samples and/or (b) primarily concerned with one particular approach of estimating the sampling uncertainty. Notable exceptions to (a) are the studies of Oki and Sumi (1994) and Steiner (1996), the former using a large dataset of gauge-adjusted radar data over Japan and the latter lots of rain gauge data from Melbourne, Florida, and especially Darwin, Australia. An exception to (b) is the study of Li et al. (1996), who compared rainfall sampling uncertainty estimates based on stationary and nonstationary rainfall models, plus the resampling by shifts method—albeit on 1 month of data from Darwin only. Much research has focused on assessing the uncertainty of rainfall averages as a function of sampling frequency for fixed space and time domains. The scaling of sampling-related uncertainty with space and time domains has received attention mostly from a theoretical perspective based on stochastic rainfall model assumptions. Similarly, the dependence of sampling uncertainty on rainfall characteristics awaits a thorough evaluation based on large amounts of data.

The extensive analyses presented here thus provide a unique basis for evaluating the sampling uncertainty behavior as a function of space and time domains, sampling frequency, and rainfall characteristics. Moreover, the results of this study enable comparison to sampling uncertainties estimated over a wide range of climatic rainfall conditions and sampling configurations. This is achieved by scaling the respective results to a common basis in terms of space and time domains, sampling frequency, and rainfall. Before we can do so, however, we need to concern ourselves with the problem of rainfall calibration first. A calibration error in rainfall could potentially affect comparisons in two different ways: (i) through errors in the estimation of the sampling uncertainty and/or (ii) the comparison of sampling uncertainties derived for various climatic rainfall regimes or observing platforms.

A rainfall calibration error will affect both the variance of the area-average rainfall and the mean rain rate. Fortunately, however, the relative sampling uncertainty, expressed in terms of the ratio of standard deviation divided by the mean, remains unaffected by a rainfall calibration error—at least when the calibration error is multiplicative in nature. Similarly, the correlation time of the area-average rainfall is not affected as well. Thus, the relative sampling uncertainties estimated by both the resampling by shifts and the Laughlin–Bell methods are unaffected by calibration error.

The relative sampling uncertainty needs to be tied to an *absolute* mean rain rate, however, in order to make it comparable to results obtained for different climate regimes or observing platforms. This is where the problem of a potential rainfall calibration error may enter. A simple back-of-the-envelope calculation shows how much difference a calibration error might cause. Let us assume that $\sigma_E/\overline{R}$ is the relative sampling uncertainty estimated for a given mean rain rate $\overline{R}$ and fixed space and time domains, and sampling frequency. Moreover, let us assume that the sampling uncertainty scales as Eq. (11) suggests, $\sigma_E/\overline{R} = \alpha\overline{R}^{-\beta}$. It can be shown then that a rainfall calibration error γ has no effect on the power factor β. Because the relative sampling uncertainties obtained for two different rainfall calibrations are identical, as demonstrated earlier, it follows that

$$\alpha\overline{R}^{-\beta} = \frac{\sigma_E}{\overline{R}} = \frac{\tilde{\sigma}_E}{\gamma\overline{R}} = \tilde{\alpha}(\gamma\overline{R})^{-\beta}. \tag{12}$$

The two multiplicative factors of the above scaling law, therefore, are related through $\tilde{\alpha} = \alpha\gamma^{\beta}$. In order to quantify this effect, let us assume a calibration error of $\gamma = 2$—radar-based rainfall estimates may easily be in

error by a factor of 2 compared to rain gauges, because of application of an inappropriate relationship between radar reflectivity and rain rate, or radar hardware calibration problems (e.g., Steiner et al. 1999). For a power factor of $\beta \sim 0.2$, as seen in the present analyses (section 3a), the effect of such a calibration error causes a difference of 15%. Note that Chang and Chiu (2001) and Bell et al. (2001) find $\beta \sim 0.3$ based on several years worth of Special Sensor Microwave Imager (SSM/I) and TRMM Microwave Imager (TMI) rainfall estimates over tropical latitudes. For a power factor of $\beta \sim 0.5$, which appears more typical for rainfall over southern Japan (Oki and Sumi 1994; see also Bell and Kundu 1996, 2000) and near Darwin, Australia (Steiner 1996), however, the calibration error will result in a 40% difference. In summary, one has to be aware of the rainfall calibration problem when comparing results of sampling uncertainties estimated for various locations and/or observing platforms. Moreover, for as long as the dependence of β on rainfall characteristics remains unknown, there is an inherent uncertainty with regard to the choice of β when scaling sampling uncertainties to a common basis.

Armed with knowledge about these caveats, let us now focus on comparing the results of the present analyses with sampling uncertainties estimated for various climatic regions. These comparisons will be limited primarily to studies concerned with infrequent but regularly timed, flush visits made by a single satellite, similar to our assumptions. Laughlin (1981), McConnell and North (1987), North and Nakamoto (1989), and Nakamoto et al. (1990), all using radar-based rainfall data collected during GATE, found sampling-related uncertainties of 8%–10% for monthly (30 day) rainfall estimated based on 12-h sampling over a squared domain with a side length of 280 km. The mean rain rate for GATE Phase I was 0.445 mm h^{-1} (Kedem et al. 1990; Bell et al. 1990). The present dataset does not contain rainfall examples of that intensity over a similar space and time domain. However, based on the median-fitted sampling uncertainty scaling law (11), the corresponding sampling uncertainty is predicted as 19.2%. Moreover, there is a 50% chance (i.e., shaded area in Figs. 6 and 7) that the true sampling error would fall within the range 14.4%–24.0%. Both, the GATE rainfall (Hudlow and Patterson 1979) and the rainfall data used in this study (Fig. 1) appear to compare favorably with contemporaneous rain gauge measurements. Thus, radar rainfall calibration errors may not explain the difference in estimated sampling uncertainty. In addition, the difference, whether the sampling uncertainty is gauged based on a scaling law (11) fitted to the results of the resampling by shifts approach (section 3a) or the results obtained by the Laughlin–Bell approach (fitted coefficients not shown), amounts to a few percent only. The difference in sampling uncertainty estimated for GATE rainfall and rainfall in the central United States, therefore, appears to be real and has to be attributed to differences in rainfall characteristics. For example, the coefficient of variation $\sigma_A/\overline{R}$ of the area-average rain rates over a 200-km domain is significantly smaller for GATE rainfall ($\sim$1.9) than for the data underlying this study ($\sim$3), as can be seen from Fig. 5 (see 30-day, 200-km panel). On the other hand, the correlation in time of GATE rainfall ($\tau_A \sim 8$ h) appears somewhat longer than for the central U.S. precipitation (Fig. 4). The observed differences in rainfall characteristics are consistent with the differences seen in sampling uncertainty between analyses based on GATE rainfall and this study.

Seed and Austin (1990), using radar information of rainfall observed in Florida during August 1987, report a sampling-related uncertainty of 22% for the 20-day rainfall accumulation over a 425-km domain based on 12-h sampling. The corresponding mean rain rate was 0.1 mm h^{-1}. Using Eq. (11) a sampling uncertainty of 22.2% is predicted for a similar configuration, with a 50% likelihood of the true value to range within 16.6%–27.8%. This excellent agreement, however, is likely to be fortuitous in light of the fact that the radar-based rainfall data used by Seed and Austin (1990) have not been calibrated with rain gauges. The coefficient of variation of approximately 2.8 and time correlation of 3 h estimated by Seed and Austin (1990) are similar to the present analyses.

For their analyses of sampling uncertainty, Li et al. (1996) used data collected during December 1989–February 1990 as part of the Down Under Doppler and Electricity Experiment (DUNDEE; Rutledge et al. 1992) by a radar located near Darwin, Australia. For a monthly rainfall accumulation (mean rain rate $\overline{R} \sim 0.1$ mm h^{-1}) over a 200-km domain, estimated based on 12-h sampling, a sampling-related uncertainty of 26% was obtained essentially independent of whether this uncertainty was estimated based on a stationary or nonstationary model, or the resampling by shifts technique. Present analyses based on using (11) suggest a sampling-related uncertainty of 32.7% ($\pm$8.2%) for a similar configuration. This is in fairly close agreement, particularly considering that the radar rainfall dataset used by Li et al. (1996) was only roughly calibrated with rain gauge information, and that the coefficient of variation of the area-average rain rates was about 2.5 and the time correlation approximately 3.5 h.

Soman et al. (1995, 1996) provide another set of analyses of radar-based rainfall data collected in January and February 1988 at Darwin, Australia. The sampling uncertainties estimated for the 18-day ($\overline{R} \sim 0.28$ mm h^{-1}, $\sigma_A/\overline{R} \sim 1.61$) and 21-day ($\overline{R} \sim 0.43$ mm h^{-1}, $\sigma_A/\overline{R} \sim 1.47$) time periods over a domain of roughly 280-km side length were approximately 32% and 25%, respectively, based on a TRMM-like ($\Delta t \sim 12$ h) sampling frequency. The sampling uncertainty estimates obtained by either the resampling by shifts method (Soman et al. 1995) or space–time spectral analyses (Soman et al. 1996) were in close agreement. These estimates compare also favorably with predictions of sampling un-

certainty for similar configurations using (11): 25.2% (±6.3%) and 21.9% (±5.5%) for the first and second phase, respectively.

4. Conclusions

The uncertainty of rainfall estimates obtained from discrete satellite sampling in space and time was assessed based on multiyear, continental-scale radar-mosaic data. Uncertainties for typical space and time domains, and sampling frequencies were evaluated. The sampling uncertainty was investigated for all combinations of 1-, 3-, 6-, 8-, or 12-h sampling of rainfall over 100-, 200-, or 500-km domains, and 1-, 5-, or 30-day accumulations. The analyses of four selected summer months represent the equivalent of 2 yr worth of analyses on a 500-km domain, 16 yr on a 200-km domain, and 64 yr on a 100-km domain. Moreover, a theoretical framework was established that enabled direct comparison of parametric and nonparametric statistical approaches to estimating the sampling-related uncertainty. In particular, results based on a statistical methodology with roots in the work of Laughlin (1981) and Bell et al. (1990) were contrasted with those obtained by a simple empirical resampling by shifts technique.

The main results of this study may be summarized as the following:

- The sampling uncertainty scales inversely with space (L) and time (T) domain size, and rainfall (R), but directly with sampling time interval (Δt). The scaling with space and time domain, and sampling frequency behaves as anticipated from previous studies. The scaling with rainfall, however, deviates significantly from the expected inverse square root behavior as predicted by simple theoretical models, which appeared to account for the results of Oki and Sumi (1994) and Steiner (1996).
- The rainfall sampling uncertainty, expressed as a percentage of the domain-average rain rate, may be characterized by a simple scaling law

$$\frac{\sigma_E}{R}100\% = 0.80\left(\frac{R_0}{R}\right)^{0.20}\left(\frac{L_0}{L}\right)^{0.70}\left(\frac{T_0}{T}\right)^{0.35}\left(\frac{\Delta t}{\Delta t_0}\right)^{1.05}, \quad (13)$$

  where $R_0 = 1$ mm h^{-1}, $L_0 = 500$ km, $T_0 = 30$ days, and $\Delta t_0 = 1$ h. Although (13) captures the main features of the central U.S. precipitation data, there is significant variability of sampling uncertainty about this simple (fitted) scaling law, some of which is certainly attributable to the great space–time variability of rainfall.
- Sampling uncertainties predicted by (13) are statistical in nature and should therefore be expressed in *probabilistic* terms. For example, based on the data examined, there is a 50% chance that the true sampling uncertainty may reside within the range of 0.75–1.25 times the value estimated by (13).
- The results of the parametric Laughlin–Bell and nonparametric resampling by shifts approaches to estimating the sampling-related uncertainty agree rather favorably, despite some appreciable variability. The differences between the two approaches highlight a sensitivity of the estimated sampling uncertainties to the choice of method. In addition, the assumptions leading to the Laughlin–Bell approximation (6) may not be valid for small T (few days or less), in which case the complete formulation (A16) would have to be used instead, as discussed in the appendix.
- A potential calibration error of the rainfall data does not affect the estimation of relative sampling uncertainty. However, an absolute calibration of the rainfall data is required in order to make the results comparable to other studies based on different climate regions and/or observing platforms. Such comparisons are highly sensitive to the accuracy of rainfall observations.
- Comparison among different land-based datasets reveals comparable sampling-related uncertainties for rainfall estimates based on discrete observations in space and time. Sampling uncertainties estimated for oceanic rainfall (e.g., GATE), in contrast, are somewhat smaller. This result is consistent with a larger variability and shorter time correlation of rainfall over land than over ocean (e.g., Ricciardulli and Sardeshmukh 2002).

Additional work is required to evaluate the relationship between rainfall characteristics and the power law of the scaling with domain-average rain rate. This will encompass analyses of rainfall data collected in a wide variety of climate regions. Moreover, future investigations may reveal that, besides the domain-average rain rate, variance and correlation time of the area-average instantaneous rain rate, there might be other descriptors of rainfall characteristics important for predicting sampling-related uncertainty. The sampling uncertainty will have to be explored also for more realistic satellite overflight patterns. And last but not least, in the ''real world,'' attaching a sampling uncertainty to satellite rainfall averages is based on the sample averages themselves, because the underlying true rainfall is unknown. This, of course, introduces additional uncertainty that needs to be quantified.

Acknowledgments. The thoughtful comments and suggestions of Gerald North of Texas A&M University and two additional reviewers (anonymous) are greatly appreciated. The paper was carefully proofread by Mary D. Steiner of the University of Pennsylvania. This study was supported by the National Aeronautics and Space Administration (NASA) Earth Science Program through Grants NAG5-7744 (James A. Smith and Matthias Steiner) and NAG5-9891 (Eric F. Wood), and the National Oceanic and Atmospheric Administration (NOAA) Office of Global Programs through Grant NA96GP0416 (James A. Smith). Thomas L. Bell's re-

search was supported by NASA's Office of Earth Science as part of the Tropical Rainfall Measuring Mission.

APPENDIX

Details of Estimating Sampling Uncertainty According to Laughlin

Some details of the derivation of the exact result for which Eq. (6) is an approximation are given here. For the first time, the validity of the assumption of neglecting the higher-order terms in the analytical expression for rainfall sampling uncertainty based on the parametric approach is explicitly evaluated. In addition, differences between the exact and approximate result that might explain slight tendencies for the resampling and Laughlin uncertainty estimates to disagree, as seen in Figs. 9 and 10, are explored.

The average squared uncertainty $\varepsilon^2(t_0)$ for a particular starting time t_0 is estimated in Laughlin's (1981) approach by writing the ensemble average in terms of the lagged correlations of the area-average rain rate $R_A(t)$, starting from the definition

$$\langle \varepsilon^2(t_0)\rangle = \langle [\hat{R}(t_0) - \overline{R}]^2\rangle \tag{A1}$$

$$= \langle [\hat{R}'(t_0) - \overline{R}']^2\rangle, \tag{A2}$$

where $\hat{R}(t_0)$ is the sample average rainfall for starting time t_0 and $\overline{R}$ is the true mean rainfall as given in Eqs. (3) and (2), respectively; and where the primes indicate deviations from the ensemble mean, $z' \equiv z - \langle z\rangle$. Equation (A2) expands to

$$\langle \varepsilon^2(t_0)\rangle = \langle [\hat{R}'(t_0)]^2\rangle + \langle \overline{R}'^2\rangle - 2\langle \hat{R}'(t_0)\overline{R}'\rangle. \tag{A3}$$

Substituting (3) into the first term of (A3), we obtain

$$\langle [\hat{R}'(t_0)]^2\rangle = \frac{1}{n^2}\sum_{i=0}^{n-1}\sum_{j=0}^{n-1}\langle R'_A(t_0 + i\Delta t)R'_A(t_0 + j\Delta t)\rangle, \tag{A4}$$

and defining the lagged covariance of $R_A(t)$ as

$$c_A(\tau) = \langle R'_A(t + \tau)R'_A(t)\rangle, \tag{A5}$$

which was assumed by Laughlin (1981) to depend only on the separation in time of the two rain rates, we can write (A4) as

$$\langle [\hat{R}'(t_0)]^2\rangle = \frac{1}{n^2}\sum_{i=0}^{n-1}\sum_{j=0}^{n-1} c_A[(i - j)\Delta t] \tag{A6}$$

$$= \frac{1}{n^2}\sum_{q=-(n-1)}^{n-1}(n - |q|)c_A(q\Delta t), \tag{A7}$$

where we have used the dependence of $c_A[(i - j)\Delta t]$ on i and j only through the difference $i - j$ to rewrite the double sum in (A6) as a single sum in (A7). Note that (A7) does not in fact depend on t_0.

Likewise, the second term in (A3) can be written in terms of $c_A(\tau)$ using the definition of $\overline{R}$ in Eq. (2) to obtain

$$\langle \overline{R}'^2\rangle = \frac{1}{T^2}\int_0^T\int_0^T c_A(t_1 - t_2)\, dt_2\, dt_1 \tag{A8}$$

$$= \frac{1}{T^2}\int_{-T}^{T}(T - |u|)c_A(u)\, du, \tag{A9}$$

where the double integral in (A8) has been reduced to a single integral by taking advantage of the integrand's dependence on the difference in the two integration times. As in the case of (A7), (A9) does not depend on t_0.

The cross term in (A3), after substitution for $\overline{R}$ and $\hat{R}(t_0)$ from Eqs. (2) and (3), becomes

$$\langle \hat{R}'(t_0)\overline{R}'\rangle = \frac{1}{n}\sum_{i=0}^{n-1}\frac{1}{T}\int_0^T c_A(t_0 + i\Delta t - t_1)\, dt_1. \tag{A10}$$

Although more complex than the previous two terms, this can be simplified considerably if we take into account at this point the resampling by shifts averaging in Eq. (5), which we approximate as a continuous average,

$$\langle \hat{R}'(t_0)\overline{R}'\rangle_{t_0} \approx \frac{1}{\Delta t}\int_0^{\Delta t}\langle \hat{R}'(t_0)\overline{R}'\rangle\, dt_0. \tag{A11}$$

We can then use (A10) and $n = T/\Delta t$ to write (A11) as

$$\langle \hat{R}'(t_0)\overline{R}'\rangle_{t_0}$$

$$\approx \frac{1}{T}\int_0^T\left[\frac{\Delta t}{T}\sum_{i=0}^{n-1}\frac{1}{\Delta t}\int_0^{\Delta t} c_A(t_0 + i\Delta t - t_1)\, dt_0\right] dt_1$$

$$= \frac{1}{T^2}\int_0^T\int_0^T c_A(t_2 - t_1)\, dt_2\, dt_1 = \langle \overline{R}'^2\rangle, \tag{A12}$$

where the last step in (A12) uses (A8). Laughlin's (1981) approach therefore gives an approximate expression for the resampling by shifts average over Eq. (A3) as

$$\langle \varepsilon^2(t_0)\rangle_{t_0} = \langle [\hat{R}'(t_0)]^2\rangle - \langle \overline{R}'^2\rangle. \tag{A13}$$

Laughlin (1981) proposed approximating the lagged covariance as an exponential,

$$c_A(\tau) = \sigma_A^2 e^{-|\tau|/\tau_A}, \tag{A14}$$

where σ_A^2 is the variance and τ_A the correlation time of the instantaneous area-average rain rate $R_A(t)$. If the assumed form of the autocorrelation (A14) is substituted into (A7) and (A9), some straightforward algebra and the summation identities

$$\sum_{q=0}^{n-1} z^q = \frac{1 - z^n}{1 - z}$$

$$\sum_{q=0}^{n-1} qz^q = \frac{z - [n - (n - 1)z]z^n}{(1 - z)^2} \tag{A15}$$

give

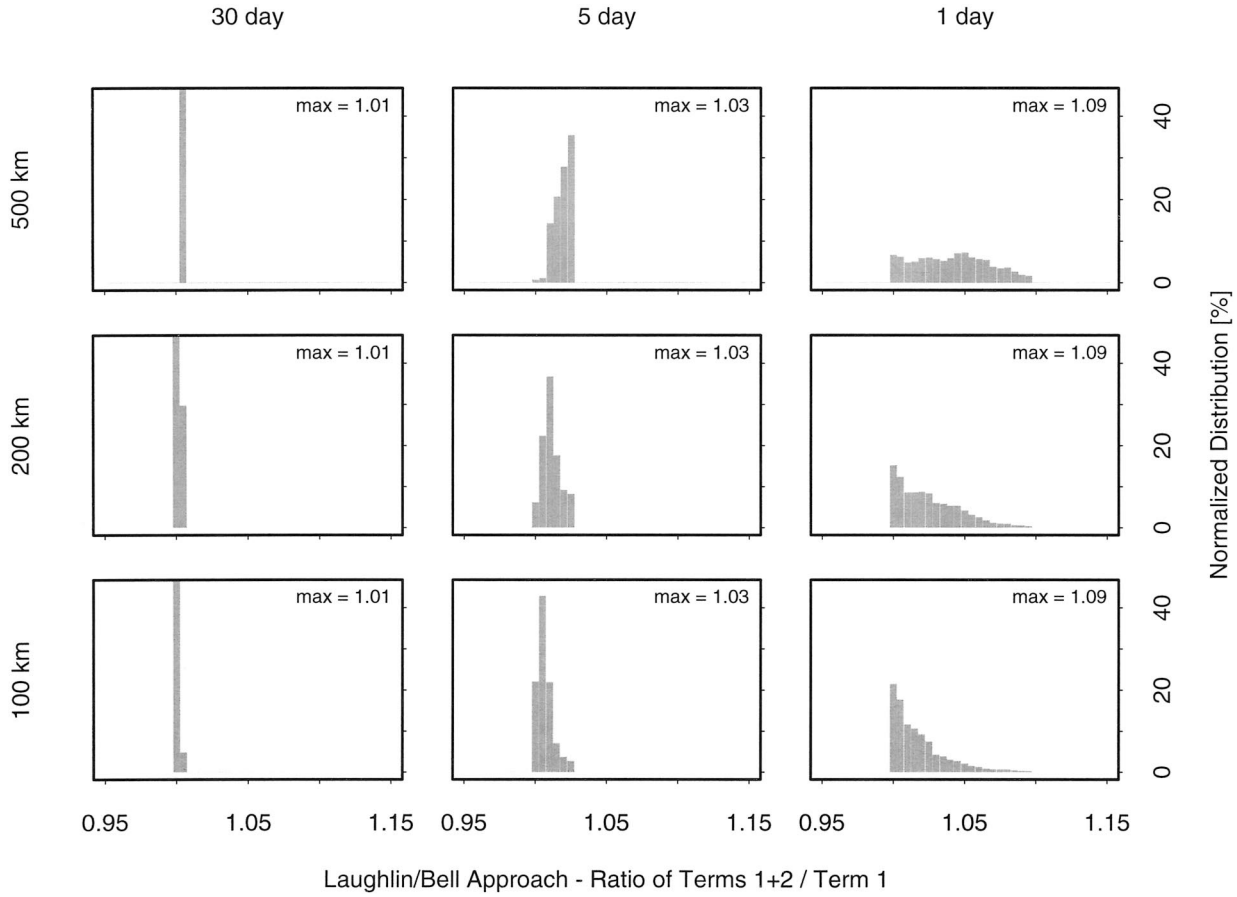

FIG. A1. Distributions of the ratio of sampling uncertainty estimated by the Laughlin–Bell approach using Eq. (A16) (i.e., including both terms c_1 and c_2) and using approximation (6) (i.e., c_1 term only). Shown are the results for the space and time domains explored based on the 4-month dataset. No distinction is made for different sampling frequencies. The distributions are normalized by their respective sample size.

$$\sigma_E^2 = \langle [\hat{R}(t_0) - \overline{R}]^2 \rangle_{t_0} = \sigma_A^2 \left\{ \frac{\Delta t}{T} c_1\left(\frac{\Delta t}{\tau_A}\right) + \left(\frac{\Delta t}{T}\right)^2 c_2\left(\frac{\Delta t}{\tau_A}\right)\left[1 - \exp\left(-\frac{T}{\tau_A}\right)\right]\right\} \quad \text{(A16)}$$

with $c_1(z)$ given by Eq. (7) and

$$c_2(z) = 2z^{-2} + [1 - \cosh(z)]^{-1}. \quad \text{(A17)}$$

Note that assumptions different from (A14) for the lagged autocovariance will result in different expressions for (A16). The term $\exp(-T/\tau_A)$ in (A16) is of order 10^{-2} or less for values of T and τ_A met here, and so can be ignored. The Laughlin–Bell approach, expressed by Eq. (6), is a good approximation to (A16) when T is large.

What is the effect of the c_2 term when estimating the sampling uncertainty using (A16) instead of Eq. (6)? The effect of including this term in the Laughlin–Bell estimates becomes noticeable for 5-day and particularly for 1-day periods, as highlighted by Fig. A1. Note that no distinction was made for different sampling frequencies, because of the small overall effect. The effect becomes more apparent with decreasing time rather than space domain. However, the maximum difference in sampling uncertainty estimates between using the c_1 term only (i.e., setting $c_2 = 0$) or using both terms c_1 and c_2 in (A16) was less than 10% for the space and time domains explored. This is clearly less than the difference between estimating the sampling uncertainty based on the resampling by shifts method and the Laughlin–Bell approach, as displayed in Figs. 9 and 10 and gauged by Tables 4 and 5. On a monthly or even weekly basis, therefore, the c_2 term may safely be ignored.

REFERENCES

Astin, I., 1997: A survey of studies into errors in large scale space-time averages of rainfall, cloud cover, sea surface processes and the Earth's radiation budget as derived from low Earth orbit satellite instruments because of their incomplete temporal and spatial coverage. *Surv. Geophys.*, **18,** 385–403.

Bell, T. L., 1987: A space-time stochastic model of rainfall for satellite remote-sensing studies. *J. Geophys. Res.*, **92D,** 9631–9643.

——, and P. K. Kundu, 1996: A study of the sampling error in satellite

rainfall estimates using optimal averaging of data and a stochastic model. *J. Climate,* **9,** 1251–1268.
——, and ——, 2000: Dependence of satellite sampling error on monthly averaged rain rates: Comparison of simple models and recent studies. *J. Climate,* **13,** 449–462.
——, A. Abdullah, R. L. Martin, and G. R. North, 1990: Sampling errors for satellite-derived tropical rainfall—Monte Carlo study using a space-time stochastic model. *J. Geophys. Res.,* **95D,** 2195–2205.
——, P. K. Kundu, and C. D. Kummerow, 2001: Sampling errors of SMM/I and TRMM rainfall averages: Comparison with error estimates from surface data and a simple model. *J. Appl. Meteor.,* **40,** 938–954.
Berg, W., and S. K. Avery, 1995: Evaluation of monthly rainfall estimates derived from the Special Sensor Microwave/Imager (SSM/I) over the tropical Pacific. *J. Geophys. Res.,* **100D,** 1295–1315.
Carbone, R. E., J. D. Tuttle, D. A. Ahijevych, and S. B. Trier, 2002: Inferences of predictability associated with warm season precipitation episodes. *J. Atmos. Sci.,* **59,** 2033–2056.
Chang, A. T. C., and L. S. Chiu, 2001: Non-systematic errors of monthly oceanic rainfall derived from passive microwave radiometry. *Geophys. Res. Lett.,* **28,** 1223–1226.
——, ——, and T. T. Wilheit, 1993: Random errors of oceanic monthly rainfall derived from SSM/I using probability distribution functions. *Mon. Wea. Rev.,* **121,** 2351–2354.
Chelton, D. B., and M. G. Schlax, 1991: Estimation of time averages from irregularly spaced observations—With application to coastal zone color scanner estimates of chlorophyll concentration. *J. Geophys. Res.,* **96C,** 14 669–14 692.
Ferraro, R., and Coauthors, 2002: NOAA satellite-derived hydrological products prove their worth. *EOS, Trans. Amer. Geophys. Union,* **83,** 429–437.
Ha, E., and G. R. North, 1995: Model studies of beam-filling error for rain-rate retrieval with microwave radiometers. *J. Atmos. Oceanic Technol.,* **12,** 268–281.
Hudlow, M. D., and V. L. Patterson, 1979: *GATE Radar Rainfall Atlas.* NOAA Special Report, Environmental Data and Information Service, National Oceanic and Atmospheric Administration, Washington, DC, 35 pp.
Huffman, G. J., 1997: Estimates of root-mean-square random error for finite samples of estimated precipitation. *J. Appl. Meteor.,* **36,** 1191–1202.
Kedem, B., L. S. Chiu, and G. R. North, 1990: Estimation of mean rain rate: Application to satellite observations. *J. Geophys. Res.,* **95D,** 1965–1972.
Kidder, S. Q., M. D. Goldberg, R. M. Zehr, M. DeMaria, J. F. W. Purdom, C. S. Velden, N. C. Grody, and S. J. Kusselson, 2000: Satellite analysis of tropical cyclones using the Advanced Microwave Sounding Unit (AMSU). *Bull. Amer. Meteor. Soc.,* **81,** 1241–1259.
Kuettner, J. P., D. E. Parker, D. R. Rodenhuis, H. Hoeber, H. Kraus, and G. Philander, 1974: GATE final international scientific plans. *Bull. Amer. Meteor. Soc.,* **55,** 711–744.
Kummerow, C., W. Barnes, T. Kozu, J. Shiue, and J. Simpson, 1998: The Tropical Rainfall Measuring Mission (TRMM) sensor package. *J. Atmos. Oceanic Technol.,* **15,** 809–817.
Laughlin, C. R., 1981: On the effect of temporal sampling on the observation of mean rainfall. Precipitation Measurements from Space, Workshop Report, NASA Goddard Space Flight Center, D5–D66. [Available from Goddard Space Flight Center, Greenbelt, MD 20771.]
Li, Q., R. L. Bras, and D. Veneziano, 1996: Analysis of Darwin rainfall data: Implications on sampling strategy. *J. Appl. Meteor.,* **35,** 372–385.
McConnell, A., and G. R. North, 1987: Sampling errors in satellite estimates of tropical rain. *J. Geophys. Res.,* **92D,** 9567–9570.
Nakamoto, S., J. B. Valdés, and G. R. North, 1990: Frequency–wavenumber spectrum for GATE phase I rainfields. *J. Appl. Meteor.,* **29,** 842–850.
Negri, A. J., T. L. Bell, and L. Xu, 2002: Sampling of the diurnal cycle of precipitation using TRMM. *J. Atmos. Oceanic Technol.,* **19,** 1333–1344.
North, G. R., and S. Nakamoto, 1989: Formalism for comparing rain estimation designs. *J. Atmos. Oceanic Technol.,* **6,** 985–992.
——, S. S. P. Shen, and R. Upson, 1993: Sampling errors in rainfall estimates by multiple satellites. *J. Appl. Meteor.,* **32,** 399–410.
Oki, R., and A. Sumi, 1994: Sampling simulation of TRMM rainfall estimation using radar-AMeDAS composites. *J. Appl. Meteor.,* **33,** 1597–1608.
Ricciardulli, L., and P. D. Sardeshmukh, 2002: Local time- and space scales of organized tropical deep convection. *J. Climate,* **15,** 2775–2790.
Rodriguez-Iturbe, I., M. Marani, P. D'Odorico, and A. Rinaldo, 1998: On space-time scaling of cumulated rainfall fields. *Water Resour. Res.,* **34,** 3461–3469.
Rutledge, S. A., E. R. Williams, and T. D. Keenan, 1992: The Down Under Doppler and Electricity Experiment (DUNDEE): Overview and preliminary results. *Bull. Amer. Meteor. Soc.,* **73,** 3–16.
Salby, M. L., 1982a: Sampling theory for asynoptic satellite observations. Part I: Space–time spectra, resolution, and aliasing. *J. Atmos. Sci.,* **39,** 2577–2600.
——, 1982b: Sampling theory for asynoptic satellite observations. Part II: Fast Fourier synoptic mapping. *J. Atmos. Sci.,* **39,** 2601–2614.
Seed, A., and G. L. Austin, 1990: Variability of summer Florida rainfall and its significance for the estimation of rainfall by gages, radar, and satellite. *J. Geophys. Res.,* **95D,** 2207–2215.
Shin, K.-S., and G. R. North, 1988: Sampling error study for rainfall estimate by satellite using a stochastic model. *J. Appl. Meteor.,* **27,** 1218–1231.
Simpson, J., R. F. Adler, and G. R. North, 1988: A proposed Tropical Rainfall Measuring Mission (TRMM) satellite. *Bull. Amer. Meteor. Soc.,* **69,** 278–295.
——, C. Kummerow, W. K. Tao, and R. F. Adler, 1996: On the Tropical Rainfall Measuring Mission (TRMM). *Meteor. Atmos. Phys.,* **60,** 19–36.
Soman, V. V., J. B. Valdés, and G. R. North, 1995: Satellite sampling and the diurnal cycle statistics of Darwin rainfall data. *J. Appl. Meteor.,* **34,** 2481–2490.
——, ——, and ——, 1996: Estimation of sampling errors and scale parameters using two- and three-dimensional rainfall data analyses. *J. Geophys. Res.,* **101D,** 26 453–26 460.
Steiner, M., 1996: Uncertainty of estimates of monthly areal rainfall for temporally sparse remote observations. *Water Resour. Res.,* **32,** 373–388.
——, and R. A. Houze Jr., 1998: Sensitivity of monthly three-dimensional radar-echo characteristics to sampling frequency. *J. Meteor. Soc. Japan,* **76,** 73–95.
——, ——, and S. E. Yuter, 1995: Climatological characterization of three-dimensional storm structure from operational radar and rain gauge data. *J. Appl. Meteor.,* **34,** 1978–2007.
——, J. A. Smith, S. J. Burges, C. V. Alonso, and R. W. Darden, 1999: Effect of bias adjustment and rain gauge data quality control on radar rainfall estimation. *Water Resour. Res.,* **35,** 2487–2503.
Weng, F., R. R. Ferraro, and N. C. Grody, 1994: Global precipitation estimations using Defense Meteorological Satellite program F10 and F11 special sensor microwave imager data. *J. Geophys. Res.,* **99D,** 14 493–14 502.
Wilheit, T. T., 1988: Error analysis for the Tropical Rainfall Measuring Mission (TRMM). *Tropical Rainfall Measurements,* J. S. Theon and N. Fugono, Eds., A. Deepak, 377–385.
Wu, D. L., P. B. Hays, and W. R. Skinner, 1995: A least squares method for spectral analysis of space–time series. *J. Atmos. Sci.,* **52,** 3501–3511.
Wunsch, C., 1989: Sampling characteristics of satellite orbits. *J. Atmos. Oceanic Technol.,* **6,** 891–907.
Zeng, L., and G. Levy, 1995: Space and time aliasing structure in monthly mean polar-orbiting satellite data. *J. Geophys. Res.,* **100D,** 5133–5142.